Multicomponent polymer systems with electromagnetic properties

Ing. Marek Jurča, Ph.D.

Doctoral Thesis Summary

Tomas Bata University in Zlín

Tomas Bata University in Zlín
Centre of Polymer Systems

Doctoral Thesis Summary

Multicomponent polymer systems with electromagnetic properties

Multikomponentní polymerní systémy s elektromagnetickými vlastnostmi

Author: **Ing. Marek Jurča, Ph.D.**

Study Programme: Nanotechnology and advanced materials (P3972)

Study Course: Nanotechnology and advanced materials (3942V006)

Supervisor: Prof. Ing. Jarmila Vilčáková, Ph.D.

Consultant: Endowed Chair and Prof. Stephen H. Foulger, Ph.D.

External examiners: prof. Ing. Petr Slobodian, Ph.D.

                     Assoc. Prof. Dr. Ing. Vladimír Pavlínek

                     Assoc. Prof. Petr Filip, CSc.

Zlín, January 2023

ACKNOWLEDGEMENTS

ABSTRACT

This work focusses on three types of electrically conductive multicomponent polymer systems: 1) nickel-filled immiscible polymer blend composites, 2) Ni-polyaniline (PANI) core-shell particles, and 3) polypyrrole (PPy) coated melamine porous structures (MS) with coprecipitated Fe_3O_4 nanoparticles.

The nickel-filled adhesive polymer composites were investigated experimentally and by numerical modelling to optimize the electrical and mechanical properties. Utilization of an immiscible polymer blend with an optimized ratio of epoxy resin (ER) and polydimethylsiloxane (PDMS) resulted in a reduction of electrical percolation threshold (EPT) from 7.9 to 3.7 vol.% Ni. The adhesion of the composite material was enhanced by 20% and the impact toughness by 75% by the addition of PDMS. Prior to the actual preparation of the composite materials, Monte Carlo and finite element method (FEM, Digimat-Fe 6.1.1) simulations were performed, which correlated well with the measured conductivity of the prepared composite materials.

The synthesized core-shell Ni-PANI particles contained 7−60 wt.% Ni. The pressure dependence of the conductivity was measured for these particles, with the particles reaching conductivities of up to 10^{-2} S/cm in the moulded form. The lower conductivity of the particles compared to pure PANI was due to a lower degree of protonation. However, compared to neat PANI, Ni-PANI particles achieved two orders of magnitude higher magnetization (M_s = 34.5 emu/g). The addition of these particles to thermoplastic polyurethane resulted in a significant increase in stiffness 13 times. Electromagnetic interference testing of these materials showed good shielding with 15% absorption and 50% reflection.

The electrical conductivity as a function of compression of the in situ synthesized MS/PPy porous structures decreased slightly by coprecipitation of Fe_3O_4 nanoparticles from 0.05 to 0.02 S/cm. However, this decrease was compensated by a dramatic increase in magnetization by 2 orders of magnitude to M_s = 12.3 emu/g, leading to an increase in microwave absorption from 50% to 75% and a decrease in transmission from 30% to 10%. Carbonization of MS/PPy with increased PPy content (27.4 wt.%) at 700 °C in an inert atmosphere was also performed, during which the porosity of the material measured by both specific surface area (300 m^2/g) and pore volume (0.25 cm^3/g) increased fourfold. The change in structure led to a drop in electrical conductivity from 0.2 to 0.03 S/cm.

ABSTRAKT

Tato práce se zabývá třemi typy elektricky vodivých multikomponentních polymerních systémů: 1) niklem plněné kompozity na bázi nemísitelného polymerního blendu, 2) Ni-polyanilinové (PANI) core-shell částice a 3) polypyrolem (PPy) potažené melaminové porézní struktury (MS) s koprecipitačně připravenými Fe_3O_4 nanočásticemi.

Adhezivní polymerní kompozity plněné niklem byly zkoumány experimentálně a numerickým modelováním s cílem optimalizace elektrických a mechanických vlastností. Využití nemísitelné polymerní směsi s optimalizovaným poměrem epoxidové pryskyřice (ER) a polydimetylsiloxanu (PDMS) vedlo ke snížení elektrického perkolačního prahu (EPT) ze 7,9 na 3,7 obj.% Ni. Přídavkem PDMS byla adheze kompozitního materiálu zvýšena o 20 % a rázová houževnatost o 75 %. Před samotnou přípravou kompozitních materiálů byly provedeny simulace pomocí metody Monte Carlo a metodou konečných prvků (FEM, Digimat-Fe 6.1.1), které dobře korelovaly s naměřenou vodivostí připravených kompozitních materiálů.

U syntetizovaných core-shell částic Ni-PANI obsahujících 7–60 hm.% Ni byla změřena závislost vodivosti na tlaku, kdy v lisované formě vodivost dosahovala až 10^{-2} S/cm. Nižší vodivost částic ve srovnání s čistým PANI byla způsobena nižším stupněm protonace. Nicméně proti čistému PANI dosahují Ni-PANI částice o dva řády vyšší magnetizaci ($M_s = 34,5$ emu/g). Přídavkem těchto částic do TPU došlo až k 13násobému nárůstu tuhosti. Testování těchto materiálů na elektromagnetickou interferenci ukázalo dobré stínění s absorpcí 15 % a reflexí 50 %.

Elektrická vodivost v závislosti na tlaku in situ syntetizovaných MS/PPy porézních struktur mírně klesla koprecipitací nanočástic Fe_3O_4 z 0,05 na 0,02 S/cm. Nicméně tento pokles byl vyvážen dramatickým nárůstem magnetizace o 2 řády na $M_s = 12,3$ emu/g, což vedlo k nárůstu absorpce mikrovlnného záření z 50 na 75 % a poklesu transmise z 30 na 10 %. Byla provedena také karbonizace MS/PPy se zvýšeným obsahem PPy (27,4 hm.%) při 700 °C v inertní atmosféře, během které vzrostla porozita materiálu měřená specifickým povrchem (300 m^2/g) a objemem pórů (0,25 cm^3/g) čtyřnásobně. Změna struktury vedla k poklesu elektrické vodivosti z 0,2 na 0,03 S/cm.

CONTENT

1. THEORETICAL BACKGROUND

1.1 Introduction to electromagnetic composites

Conductive and magnetic polymer composites (CPCs; MPCs) attract the scientific community as well as industry for their potential applications in various fields of science and technology: antistatic materials, anticorrosion coatings, electromagnetic shielding and light emitting devices, electromagnetic wave absorbers etc. [1] Composite material consisting of an insulating polymer matrix becomes electrically conductive if a conductive path is created by conductive filler. A conductive path may be a complex multi-scale structure consisting of interconnected particle aggregates forming infinite clusters. Such aggregates hold by particle-particles interactions, their size can be visualized by scattering electron microscopy and evaluated by aggregation number N_{agg} [2]. Percolation theory is relatively successful in predicting the general conductive characteristics of CPCs materials. The distance of conducting particles converges to a percolation distance where the transfer of charge carriers between them is probable. The insulator-conductor transition's concentration occurs is called the electrical percolation threshold (EPT) [3, 4]. There have been many attempts to reduce the percolation threshold of CPCs using fillers of different sizes and shapes [5] such as spherical (carbon black (CB) or metal powder [6, 7]), fibrous (carbon nanotubes (CNT) [8]), flakes (graphite [9]) and asymmetric – arbitrary ellipsoid (Ni [10]). According to Scher-Zallen, the percolation limit, calculated for a model system of randomly localized conducting spherical particles in a 3D matrix, is around 16 vol.% [11]. To effectively reduce the percolation threshold, a novel hierarchical structure, i.e., double percolation threshold (DPT) was utilized [6, 7, 12]. In the classic double percolation structure, so called percolation-within-percolation [7], the conductive fillers are selectively located in one phase of the co-continuous polymer blend. It means that the fillers only need to form a percolated conductive network throughout their hosting phase [12].

The particle localization in immiscible polymer blends is heterogeneous, often with the particles preferentially localized only in one phase or on the interphase of two particles. This happens due to a different strength of interactions between particles and immiscible polymer chains, which can mathematically be described as the balance of interfacial energies. Generally, polymer chains are losing conformational entropy if they stretch around solid particles causing an increase of entropic over enthalpic interactions. For the systems with similar interfacial energies, the particle arrangement can be also given by the melt viscosity effect of the polymers [13].

Many attempts to predict the percolation threshold of polymer composites have been made; however, each model has limitations and simplified assumptions (i.e., monodisperse particle size distribution [11]. However, for systems exhibiting

a double percolation threshold, there are not any appropriate models and thus numerical modelling is the only option for predicting the polymer composite electrical conductivity, due to the complicated multi-phase morphologies [14]. The Monte Carlo (MC) simulation is an effective method to simulate the random dispersion of conductive fillers in the matrix, which is usually used to analyse the electrical percolation of composites, and get rich achievements [9]. Therefore, numerical simulations which are now available by means of the Monte Carlo method, random sequential addition and computational homogenisation are applied to study percolation threshold concentration of CPCs [15, 16]. E.g., Dalmas et al. [15] simulated the percolation threshold for fibrous CNT, while Xiong Zhuo-Yue et al. [16] investigated a hybrid system containing CNT and CB. Musino et al. [2] used computational modelling to study rheological percolation threshold of spherical silica particles.

1.2 Percolation threshold

A composite material consisting of an insulating polymer matrix is electrically conductive if a conductive path created by conductive filler reaches a critical value, i.e., the EPT. Thus, the concentration of conductive particles is a crucial factor influencing the electrical conductivity of epoxy polymer composites. Percolation theory is relatively successful in predicting the general conductive characteristics of CPCs materials [3, 4]. According to Scher-Zallen, the percolation limit, calculated for a model system of randomly distributed conducting spherical particles in a 3D matrix, is around 16 vol.% [11]. Geometrical factors also influence the EPT and there have been many attempts to reduce the percolation threshold of CPCs using fillers of different sizes and shapes [5]. Other important factor affecting electrical conductivity is quality of distribution and dispersion of the filler inside the polymer matrix. Filler distribution might be improved by a coating resulting in lower EPT; however, this might lead to a decrease in overall conductivity [8]. Another main factor influencing EPT is presence of other components in the mixture, either the second polymer phase or the other filler in the composite systems. For the matrices formed by immiscible polymer blends, the fillers are usually dispersed only in one polymer component. In such case the EPT is lowered proportionally to the amount of the second polymer phase. However, by a suitable choice of polymer blend and filler, it is possible to create a polymer composite with the co-continuous polymer blend as a matrix with conductive filler located almost exclusively on the polymer-polymer interphase lowering EPT even further [17]. Utilization of the second non-conductive filler has similar effects as second polymer phase [18]. However, the utilization of two conductive fillers, so called hybrid composite system, usually leads to a drastic decrease in EPT at the cost of a decrease in conductivity. One of the fillers (typically metal particles) exhibit high both conductivity and EPT while the second filler (typically carbon structures) has lower both conductivity and EPT. As a result, the metal particles

are interconnected with a carbon structure. Thus, the final EPT and conductivity of the hybrid composite are determined by the ratio of polymer fillers [19].

According to percolation theory, the conductivity of polymer composite material bellow EPT can be calculated as:

$$\sigma = \sigma_m(\rho_c - \rho)^s \tag{1}$$

where σ is the conductivity, σ_m is the conductivity of matrix, ρ_c is the percolation threshold volume concentration, ρ is the conductive filler volume concentration and s is the parameter. After reaching the percolation threshold, when the conductive paths are established, conductivity can be described as:

$$\sigma = \sigma_f(\rho - \rho_c)^t \tag{2}$$

where σ_f is the conductivity of matrix and t is the parameter.

1.2.1 Electromagnetic shielding effectiveness

Electromagnetic radiation shielding is one of many applications of composite materials and conducting polymers [20]. The reduction of radiation transmission is obtained either from increased radiation absorption or reflection. Electrically conducting polymers and composites provide both radiation reflection and (to a lesser extent) absorption, proportional to the electrical conductivity of the material [21]. Conducting polymers have been also often used for the surface modification of various supports to achieve good shielding efficiency [22]. Especially coated sponge-like materials with high values of electromagnetic shielding are valued for their low density. The most important frequency region for practical applications is 1–12 GHz in the microwave region, since the majority of the current communication and information transfer systems use it for operation.

The total shielding effectiveness SE_T for shielding materials is given as [23]:

$$SE_T = SE_A + SE_R + SE_M \tag{3}$$

where SE_A, SE_R, and SE_M are the partial shielding efficiencies related to absorption, reflection, and multiple reflections, respectively. The term related to multiple reflections and scattering SE_M can be neglected for $SE_T < 20$ dB.

The total efficiency SE_T is evaluated by using scattering parameters determined from a vector network analyser, S_{11} denotes the forward reflection coefficient and S_{21} the reverse transmission coefficient. They provide a quantitative assessment of the applicability of the individual materials in electromagnetic radiation and refer to a specific thickness. Usually, it is more convenient to discuss electromagnetic shielding in the terms of reflectance (R), absorbance (A), and transmittance (T) as percentage values rather than in the terms of SE parameters. Energetic RAT parameters calculated from attenuation can be calculated as:

$$T = 10^{\frac{S_{21}}{10}} \tag{4}$$

$$R = 10^{\frac{S_{11}}{10}} \tag{5}$$

$$A = 1 - R - T \tag{6}$$

For the sake of completness it should be noted that the efficiencies SE_A and SE_R are linked to the transmittance T and reflectance R:

$$SE_R = 10 \log\left(\frac{1}{1-R}\right) \tag{7}$$

$$SE_A = 10 \log\left(\frac{1-R}{T}\right) \tag{8}$$

1.2.2 Epoxy resin/rubber polymer blends

The usage of rubber inclusion into epoxy resin was first proposed by McGarry, Willner and Sultan in the late 1960s and early 1970s. They used carboxyl-terminated acrylonitrile-butadiene rubber (CTBN) to enhance the fracture toughness of epoxy resin (ER) with negligible losses in thermal and other mechanical properties [24]. This was the origin of research on rubber-enhanced epoxy materials [25]. Since the 1970s many blends with ER were proposed, for instance: hydroxyl-terminated butadiene rubber [26], CTBN [27], styrene-butadiene rubber [28], acrylic rubber [29], nature rubber [30], acrylonitrile-butadiene rubber [31], Polydimethylsiloxane (PDMS) [32]. The percentage content of rubber/plastic inclusion varies from ones percent [26] up to 50% [29] but commonly 10–20% is used [30, 33].

Mechanical properties usually follow the trend, where impact strength as a function of weight/volume percentage has a local maximum and the Young modulus decreases slightly at low concentrations and significantly at higher concentrations. Therefore, optimal content has to be found [32, 33, 34]. An increase in impact resistance might be 10% [33], 80% [34] and even 110% [35] depending on the types of materials and compatibility between ER and rubber.

1.3 Computer modelling

The probability of the formation of a conductive path in the composite can be simulated by the three-dimensional continuum MC method [36, 37]. The MC model is based on the cubic relative volume element (RVE) with edge length L_{RVE} filled with randomly localized spherical conductive particles and nonconductive matrix [36]. Typically, composite materials generated through MC are used in the calculations of electrical conductivity by FEM. The FEM is based on a discretization of the volume continuum (via mesh generation) into finite smaller segments which are calculated separately [36, 38]. The computational homogenisation technique assumes the material to be sufficiently homogeneous at the macro-scale but heterogeneous at the micro-scale due to the existence of inclusions.

1.4 Polymer coatings

1.4.1 Polymer coated metal particles

Hybrid organic/inorganic conducting and magnetic materials are of interest both from the academic point of view and for application in various directions. Polymer coated metallic particles are often referred to as core-shell particles. Special attention has been paid to the organic component that was represented by a conducting polymer, such as polyaniline (PANI) [39], which also improves the composite processing. The inorganic part may display both electrical and magnetic properties. Nickel [40], iron [41] or various iron oxides [42] and ferrites [43] can be introduced as the examples. Electromagnetic interference shielding represents probably the most widely studied field where both the conductivity and magnetic properties play important roles [40, 44, 45].

The range of potential applications of composites combining the conducting and magnetic components extends far beyond electromagnetic interference applications. Considering only hybrid Ni-PANI systems, typical applications as electrode materials [46] rely on electrical or electrochemical properties. The electrocatalysis of hydrogen evolution reaction [47] or the use in supercapacitor electrodes [48] are other examples. Magnetic properties of nickel in the composites have also been exploited. Hybrid adsorbents of environmental pollutants, e.g., organic dyes of heavy-metal ions [46, 49] or photocatalysts of dye decomposition have been reported in the literature [50]. Such composites are conveniently separable using a magnetic field. Similarly, the magnetorheological characteristics of suspensions are controlled by an external magnetic field [41].

The Ni-PANI hybrids of the above type have been prepared by the electrochemical deposition of Ni on PANI [47] or reduction of nickel(II) ions with ethylene glycol [50, 51]. A reverse strategy is illustrated by the in-situ coating of Ni foam with PANI [45] or electropolymerization of aniline at such macroporous substrate [48]. The similar deposition of PANI on Ni-coated carbon fibres also belongs to this category of preparations [44]. Finally, PANI and Ni particles can be simply mixed together with some additives [43].

1.4.2 Polymer coated porous structures

Magnetic hydrogels and sponges that incorporate magnetic particles have become of interest especially in biomedical applications [52]. Such composite materials can be used as drug carriers with a tunable release by an external magnetic field. The system is composed of (1) a carrier sponge that provides macroporous mechanical support, and (2) a magnetic component, typically represented by iron oxides, that affords an attractive response to the external magnetic field. Such macroporous materials are referred to as ferrosponges [52] and they can contain various paramagnetic or superparamagnetic components. They are not limited to ferromagnetic ones as the ferrosponge name may suggest.

To this structure; however, (3) another component can be added. A conducting polymer providing electrical, electrochemical, responsive or other value-added properties can be introduced.

The routine preparation of a composite has proceeded as a rule in two steps [53]: (1) In the standard approach, magnetite was prepared at first. The coprecipitation method using the mixture of iron(II) and iron(III) chlorides in ammonia solution is the most common [44]. Fe_3O_4 may be generated in particulate form as a colloid stabilized by surfactants or water-soluble polymers that afford the control of particle size and colloidal stability of magnetite particles. (2) In the second step, the oxidation of pyrrole with iron(III) chloride [53], ammonium peroxydisulfate [54] or by electropolymerization [55] to PPy took place in magnetite presence. The process resulted in a magnetite core–polypyrrole shell structures Fe_3O_4-PPy [55, 56].

Both steps can be also reversed. (1) When pyrrole was oxidized to polypyrrole with excess iron(III) chloride, only a part of the oxidant converted to iron(II) chloride [53]. In a more complex approach, iron(II) chloride along with pyrrole generated iron(III) ions were used as an oxidant of pyrrole to polypyrrole [44]. (2) As the system contained both the iron(II) and iron(III) ions, the magnetite was produced after the addition of ammonia in the second step which resulted in decoration of polypyrrole with magnetite particles. Because polypyrrole produced in the first reaction need not be separated before the addition of ammonia, such synthesis is usually referred to as "one-pot".

Melamine sponge (MS) is a macroporous material based on a melamine-formaldehyde network containing some bisulfite moieties [57]. Melamine alone is an organic compound, rich both in nitrogen and carbon, representing a suitable precursor for carbonization. It has been exposed to elevated temperatures in an inert atmosphere to obtain materials that were regarded as carbons [58, 59], nitrogen-containing carbons [59], or products close to carbon nitrides [60]. Except for some shrinkage, the macroporous morphology of the sponges was preserved after carbonization [59], but the mechanical properties were relatively poor. Conducting polymers, such as PANI and PPy, are similarly composed mainly of carbon and nitrogen atoms. They have been used frequently for the preparation of nitrogen-enriched carbons by exposure to elevated temperature in an inert atmosphere [61]. The carbonization of various polypyrrole nanostructures-globules, nanofibers and nanotubes-provides nitrogen-containing carbons of various morphology [62] with conductivity at the semiconductor level. The general features of morphology do not change after carbonization and, for example, polypyrrole globules or nanotubes convert to nitrogen-enriched carbon analogues [62, 63].

2. AIMS OF THESIS

Based on the previous literature survey, the main aim of this work was the development of multicomponent polymer composite materials using metal particles and/or conductive polymer coatings and the investigation of their electromagnetic properties for applications such as conductive coatings and electromagnetic shielding devices with a focus on mechanical properties. The accomplishment of the aim was outlined in the following tasks:

a) Development of an immiscible polymer blend suitable as a matrix for Ni composites with enhanced mechanical properties.

b) Preparation of polymer composite samples with selective localization of the conductive filler in continuous polymer phase in order to effectively reduce EPT and increase electrical conductivity.

c) Computational simulation of polymer composites based on immiscible polymer blend filled with Ni particles by the Monte Carlo method. Electrical conductivities of simulated composites in relative volume elements were calculated by the finite element method. Theoretical calculations of polymer composites dielectric and magnetic properties using effective medium theories.

d) Analysis of dielectric and magnetic properties of prepared polymer composites. Comparison of theoretical and experimental results.

e) Development of synthetic route for conductive core-shell Ni-PANI particles. Analysis of DC conductivity changes during compression, magnetostatic hysteresis curves and spectroscopy spectra of prepared Ni-PANI particles.

f) Preparation and study of mechanical properties and electromagnetic shielding interference of polymer composite samples filled with Ni-PANI particles.

g) Development of suitable polymer coating based on PPy for melamine sponge in order to create a conductive lightweight porous structure. Study the properties of these materials and seek further possibilities to improve the electromagnetic properties.

i) Deposition of ferromagnetic nanoparticles on MS/PPy porous structures to obtain magnetic conducting structures with an application for electromagnetic shielding.

j) Carbonization of porous MS/PPy materials in order to obtain conducting structures with extremely low density followed by an analysis of dc conductivity and mechanical properties.

3. EXPERIMENTAL SECTION

3.1 Materials

Common applications of electromagnetic composite materials are anti-static/conductive coatings, the alternative to soldering – conductive glues, and electromagnetic shielding devices. For all these applications, thermosets are usually used as a matrix. Epoxy resins (ER) are simple to work with, yet their performance considering thermal or mechanical properties is better compared to other options like unsaturated polyester resins. However, the drawback of ER is its brittleness. This can be improved by the addition of a second polymer phase as we showed in our study [64]. An excellent conductive filler is carbonyl nickel because it can be obtained in the form of hedgehog-like particles with a high specific surface. Soft ferromagnetic Ni is also suitable for electromagnetic shielding applications. As discussed above, the polymer blend morphology plays an important role in the electrical properties of composites. In our work, we used the DPT approach, where thermoset ER is a continuous phase with the inclusion of spherical elastomer particles, the so-called sea island structure.

Bisphenol A diglycidyl ether (DGEBA) used as an epoxy resin (ER) was cured by an aliphatic amine, diethylenetriamine (DETA). For blending was used vinyl-terminated polydimethylsiloxane (PDMS). Dicumyl peroxide (DCP) was used as a free radical initiator. All chemicals were purchased from Sigma Aldrich (USA) with a purity > 90%. Carbonyl nickel (Ni) (Goodfellow, GB) with purity 99.8% was used as a conductive filler with magnetic properties. The particle size distribution was studied by Laser diffraction. The particle size distribution was described by a normal distribution with a mean particle diameter of 5.5 μm and a standard deviation of 1.8 μm. This result is in good agreement with scanning electron microscopy SEM measurements (Figure 1) and with the data of the particle manufacturer (Goodfellow Ltd.), which states their size in the range of 2–7 μm. The FCC (face-centred cubic) Ni powder with initial relative permeability $\mu_i \approx 49.5$ has a saturation 50 emu/g, retentivity 2.1 emu/g and coercivity 39 Oe.
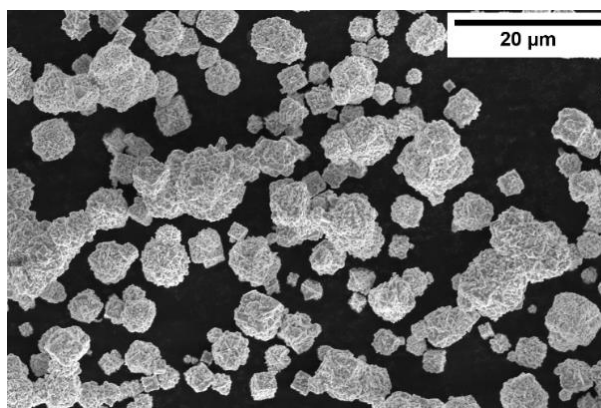

Figure 1: SEM micrograph of Ni filler.

PANI coating of Ni particles was performed in an aqueous solution of aniline hydrochloride (Sigma Aldrich, USA) and ammonium peroxydisulfate (Lach-Ner, CZ). Ni-PANI fillers were added to the matrix of thermoplastic polyurethane (TPU) Estane 58271 (The Lubrizol Corporation, USA).

Aqueous solutions of pyrrole and iron(III) chloride were used for the coating of open-cell macroporous melamine/formaldehyde (MS) Basotect sponges (BASF AG, Ludwigshafen, Germany). The solution of iron(II) chloride, iron(III) chloride and ammonium hydroxide was used for the preparation of magnetite (Fe_3O_4) particles. All above mentioned chemicals were reagent grade > 98% (Sigma Aldrich, USA).

3.2 Sample preparation

3.2.1 ER/PDMS blend preparation

The compounding of polymer matrix was investigated in other studies [64, 65]. The polymer blend was prepared by stirring DGEBA, PDMS (10–30 wt.%) and DCP (0.5 wt.%) at 300 rpm under nitrogen atmosphere for 2 hours at 130 °C. This mixing procedure resulted in the cross-linking of PDMS and improvement of the interphase between ER and PDMS phase leading to spherical particles.

3.2.2 Fabrication of ER/PDMS/Ni composites

The magnetic filler – Ni (10–80 wt.%, 1.5–33 vol.% respectively) was added to this blend after cooling the blend down to room temperature. The mixture was stirred again at 80 °C for 30 minutes and an equimolar amount of DETA was added after cooling the mixture to room temperature. The mixture was pre-cured by stirring at 50 °C for 10 minutes before casting to preheated mould (70 °C). The material was cured at 100 °C for 30 minutes and after removing from the mould, post-curing (and also cross-linking of PDMS) at 140 °C for 1 hour was done. The samples were slowly annealed at an oven to 30 °C before testing to avoid any potential freeze stresses [66].

3.2.3 Preparation of Ni-PANI particles

Ni powder was added to a freshly prepared aqueous mixture used for the preparation of PANI (0.1 M aniline hydrochloride, 0.125 M ammonium peroxydisulfate). Aniline hydrochloride and peroxydisulfate were separately dissolved in the same volume of distilled water. Both solutions were mixed at room temperature, Ni was added, and the mixture was gently stirred with a mechanical stirrer. After 1 h the solids were separated by filtration, rinsed with 1 M hydrochloric acid, followed by ethanol and dried in air [67].

3.2.4 Preparation of TPU/Ni-PANI composites

For the electromagnetic interference shielding, Ni-PANI hybrids were mixed with TPU in a micro compounder (Xplore Instruments BV, The Netherlands) with

a capacity of 5 cm^3. Prior to mixing, TPU was dried at 90 °C for 12 h. The materials were melt-mixed using 100 rpm speed at 150 °C for 5 minutes to achieve good dispersion of the Ni-PANI filler at 60 wt.% content [67].

3.2.5 Preparation of MS/PPy/Fe$_3$O$_4$ structures

The melamine sponge (MS) was immersed in a freshly prepared aqueous mixture of 0.05 M pyrrole and 0.25 M iron(III) chloride hexahydrate pre-cooled to 5 °C. The sponge was briefly gently squeezed to replace the air in the pores with the reaction mixture and the polymerization of pyrrole was let to proceed for 30 min. PPy-coated sponge still swollen with the solution of residual reaction mixture containing iron(II)/iron(III) chlorides was transferred to excess 1 M ammonia solution and left for 1 h to allow for the formation of magnetite nanoparticles. The composite MS/PPy/Fe$_3$O$_4$ was rinsed with water, immersed in ethanol in order to remove soluble low-molecular-weight residues and any free particles, and subsequently dried [21].

3.2.6 Preparation of MS/PPy carbonized structures

The preparation of MS/PPy sponges is similar as in 3.2.5 with only difference the molar ratio of pyrrol and iron(III) chloride being 2.5. The polymerization of pyrrole was complete within several minutes but the sponges were left in the reaction medium at rest for 1 h. The sponges were then transferred into an excess of 0.2 M hydrochloric acid and washed followed by washing in ethanol and drying in open air. The content of PPy was calculated from the mass increase.

The MS/PPy were subsequently placed in a tube furnace GSL-1600X-50-UL (MTI Corp., USA) and heated under an argon atmosphere at a 3 °C/min rate to target temperature up to 700 °C. After 10 minutes, the sponges were cooled to room temperature at the same rate a 3 °C/min. The difference between the original and residual weight of sponges after the exposure, was determined [68].

3.2.7 Characterization techniques

Prepared materials were characterized by instrumental techniques available at CPS:

ATR FTIR spectra of the powdered samples were analysed using Nicolet 6700 spectrometer (Thermo-Nicolet, USA) using a reflective ATR extension GladiATR (PIKE Technologies, USA) with diamond crystal.

Elemental composition was determined using a Perkin Elmer 2400 Series II CHNS/O Analyzer.

Phase morphologies of freeze-fracture surfaces of ER/PDMS/Ni polymer composites were investigated by a NovaNanoSEM 450 scanning electron microscope (FEI Company, The Netherlands) at an accelerating voltage of 5 kV in topographical SE (Secondary electrons) imaging mode and 15 kV in material

contrasting BSE (Backscattered electrons) operating mode. The morphology of PPy-Ni powders and sponges was assessed with a scanning ultra-high-resolution electron microscope MAIA3 Tescan.

The *I-V* characteristics were measured in the two-point setup using electrodes of cylindrical shape (d = 16 mm) with a programmable electrometer (Keithley 6517 A, USA). Four-point method (developed by Van der Pauw [69]) was used for the measurement of samples with conductivity higher than 10^{-3} S/cm. The dependence of resistivity of powder has also been characterized by van der Pauw method in dependence on applied pressure in a cylindrical glass cell with 10 mm inner. The powder was placed between an insulating support and a glass piston carrying four platinum/rhodium electrodes on the perimeter of its base. The experimental set-up included a current source Keithley 220, a Keithley 2010 multimeter and a Keithley 705 scanner with a Keithley 7052 matrix card. The pressure was controlled with a L6E3 load cell (Zemic Europe BV, The Netherlands).

Dielectric and magnetic properties were studied on a broadband dielectric spectrometer (Novocontrol) in the frequency range (10^{-1}–10^6) Hz, RF impedance/material analyser (Agilent E49991A) (10^6–10^9) Hz and waveguide analyser vector network analyser (Agilent N5230A) in S, C, J and X bands (2.45×10^9–12.4×10^9) Hz. Samples (cylinders, toroids and plates) were prepared according to instrumental specifications.

3.3 Modelling

3.3.1 General description

MC model was used for the simulation of the 3D composite systems in the cubic periodic RVE with an edge length L_{RVE} = 200 μm. Epoxy composites were simulated as a composition of epoxy resin (continuous phase) and non-intersecting inclusions which geometrical and material properties are defined via parameter adjustment (size distribution, shape, orientation, conductivity). Periodic boundary conditions were chosen to eliminate the boundary effect. To simulate a composite with non-conductive spherical particles (PDMS), firstly non-conductive inclusions with a normal distribution, with a mean diameter d = 32 μm and a standard deviation σ = 8 μm were generated. Afterwards the conductive Ni particles approximated as spheres with a normal diameter distribution with d = 5.5 μm and σ = 1.8 μm were generated (Figure 2). It was assumed, that Ni is not penetrating into the non-conductive inclusions of PDMS (as follows from Young's eq. (7)), as was proved in SEM images (Figure 3). The rest of the space was filled with epoxy resin which was considered perfectly bonded.

3.3.2 Modelling of growth of the aggregates

The probability of the formation of a conductive path in the composite was simulated by the three-dimensional continuum Monte Carlo method based on the cubic RVE that is filled with randomly localized spherical conductive particles and non-conductive matrix. Hard Ni particles are set as non-intersecting and hence, the particle contact is very improbable. Therefore, the contact of the particles is achieved by increasing the radius of all conductive inclusions by coating with the same thickness (*t*). A group of particles that are electrically connected shall be called aggregate. The conductive particle is considered to participate in the aggregate if the coating of the particle intersects with the coating of any other particle of this aggregate (algorithm searches for particle-particle distance ≤ *2t*). One possible evaluation method of the particle configuration produced by the simulation is the aggregation number (N_{agg}) which is the number of particles in aggregate, as discussed by Musino et al. [2]. The first moment of N_{agg} distribution is the average aggregation number, $\langle N_{agg} \rangle$; the second moment, $\langle N_{agg}^2 \rangle$, serves to express the width of the distribution. It is convenient to express the size of aggregates (*SoA*) in the term of the ratio of these moments:

$$SoA = \frac{\langle N_{agg}^2 \rangle}{\langle N_{agg} \rangle} \tag{9}$$

which is sensitive to the largest aggregates formed at the simulation and neglects isolated particles and small aggregates.

3.3.3 Modelling of electrical conductivity

In this research, the RVE method with particle inclusions is used to predict the percolation behaviour of ER/PDMS/Ni composites. Epoxy resin composites with PDMS and Ni particles were created using the Digimat-FE 6.1.1 program (e-Xstream Engineering, Louvain-la-Neuve, Belgium). The electrical conductivity was evaluated by FEM using the Digimat software [37]. FEM is based on a continuum form of Ohm's law.

A voxel mesh (1 μm side) was generated inside RVE containing microstructure generated by MC [36]. The electrical conductivity of Ni particles, Ni coating and non-conductive polymer blend ER/PDMS was set as 10^3, 1 and 10^{-12} S/cm, respectively. These systems were tested at voltage 1 V and from the *I-V* characteristic curve was calculated conductivity (ten times for each concentration). To verify these results, polymer composites were prepared and measured. In Figure 2 there are depicted simulations of polymer composites containing an increasing amount of PDMS at percolation concentrations of Ni particles (grey conductive paths). The amount of Ni particles at EPT, effectively the Ni concentration is decreasing with increasing amount of PDMS.
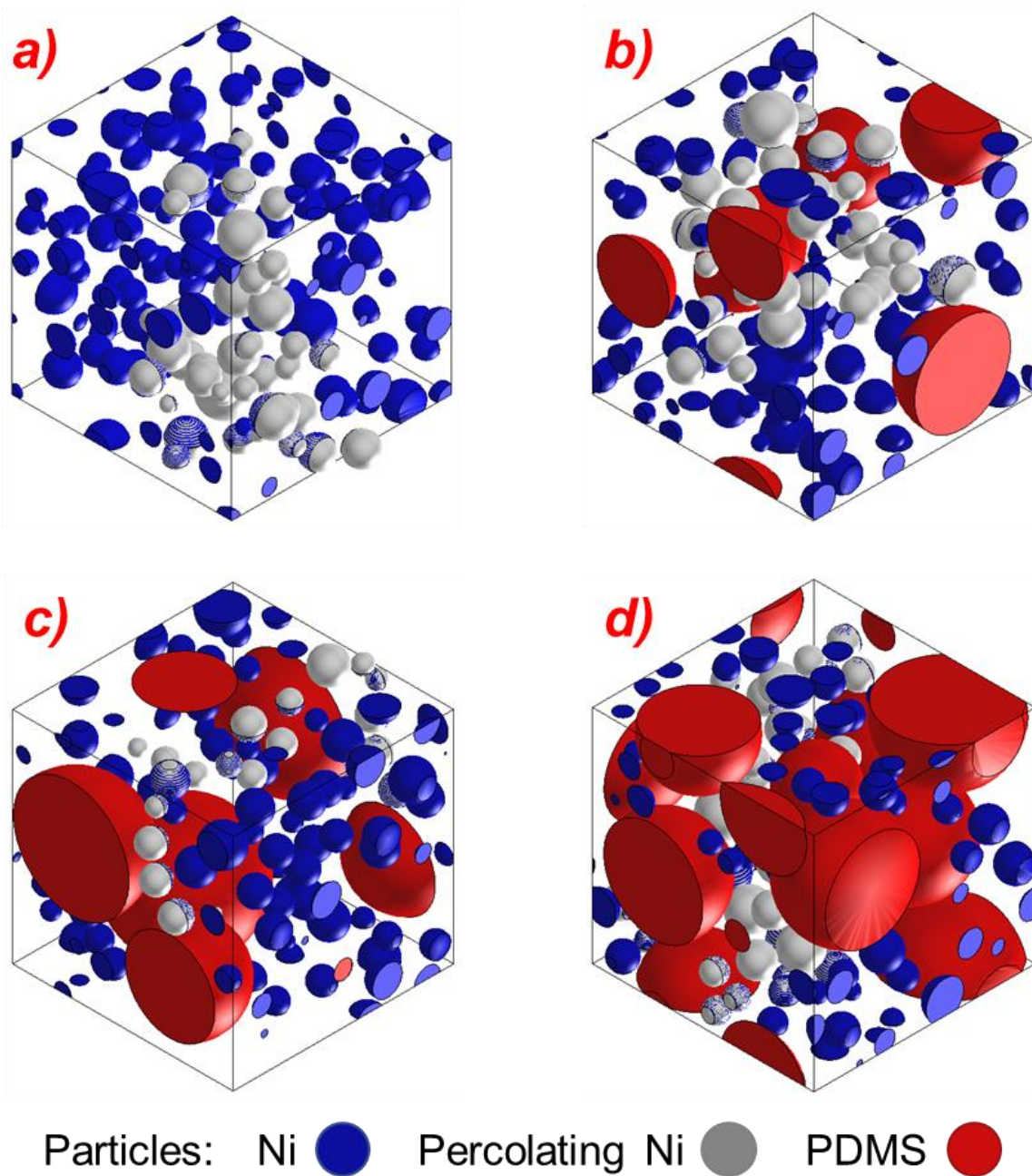
*Figure 2: The simulations reaching percolation threshold: a) ER/Ni,
b) ER/PDMS10/Ni, c) ER/PDMS20/Ni, d) ER/PDMS30/Ni [66].*

4. RESULTS AND DISCUSSION

4.1 ER/PDMS blend

4.1.1 Morphology

Immiscible polymer blend ER/PDMS forms sea island structure with continuous ER phase and spherical domains of PDMS. The observed size distribution is from 15 to 55 μm as shown in our previous studies [64, 65].

4.1.2 Mechanical properties

Mechanical properties of polymer blends prepared by the original procedure [64] led to samples with high values of Charpy impact strength. However, this procedure was further improved by modification of temperature setting and significant decrease of DCP content to 0.5 wt.% which led to impact strength of ER/PDMS10/DCP0.5 (1.8 ± 0.2) J/cm^2. Moreover, this modification of technology enabled the preparation of polymer blends with higher PDMS content (up to 30 wt.%) [66].

4.2 ER/PDMS/Ni composites

4.2.1 Morphology

In Figure 3, a series of SEM images are presented to show the morphologies of the multiphase ER/PDMS polymer blends filled with Ni. The fractured surface of all modified epoxy-based composites showed a three-phase morphology with a rigid continuous phase and a dispersed elastomeric phase of isolated spherical particles of PDMS with the typical sea-island structure of the size 15–55 μm.
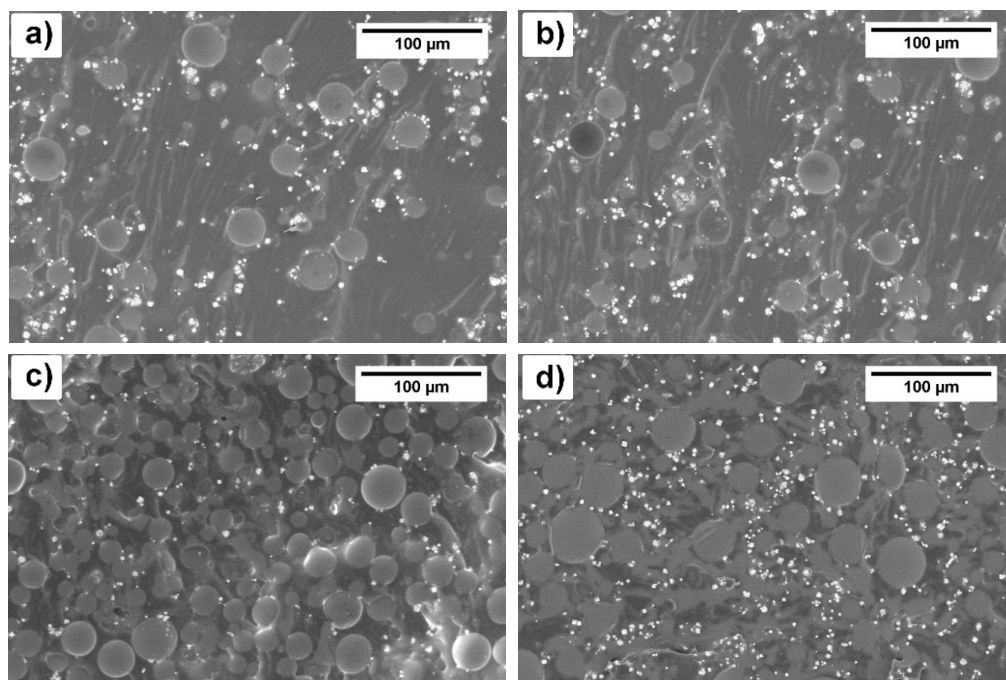

Figure 3: SEM micrographs of polymer composites: a) ER/PDMS10/Ni3, b) ER/PDMS10/Ni11, c) ER/PDMS30/Ni3, d) ER/PDMS30/Ni11 [66].

4.2.2 Computational modelling – growth of aggregates

The value of *SoA* calculated by eq. (9) ranges from 1 implying all particles are isolated to a maximum (= number of particles in the RVE). In terms of percolations, the significant size of the aggregate emerges if the largest aggregate penetrates through the whole sample, thus the diameter of the aggregate is equal to the size of the simulation RVE: $d_{agg} = L_{RVE}$. The fractal model of spheres, as presented by Musino et al. [2], predicts that such a critical aggregate occurs at *SoA* ~ 1,000 for our system ($L_{RVE} = 200$ μm, $d_{Ni} = 5.5$ μm). Figure 4 presents the dependence of *SoA* on the volume concentration of nickel for different coating sizes.

Figure 4a shows that with increasing coating size, the size of the aggregates increases dramatically, approaching a limit which is the number of particles in the system. The indicated *SoA* ~ 1,000 is the critical size of aggregate which is penetrating through the entire simulated RVE, which roughly corresponds to the percolation concentration. By comparing to the EPT, which was found to be 7.9 vol.% (Figure 5), the thickness of the coating was found to be close to 1.95 μm.
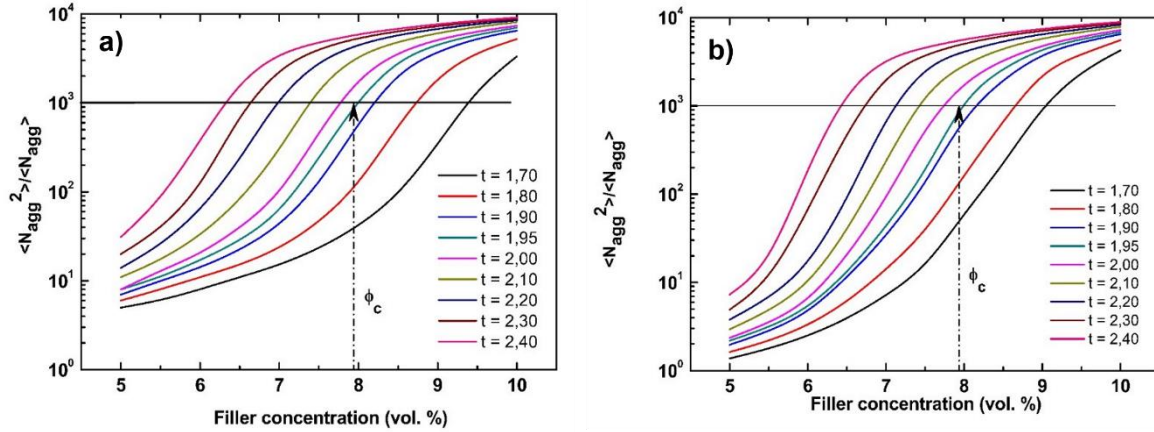

Figure 4: SoA determined from aggregation number (N_agg) distribution obtained by Monte Carlo simulation for a) ER/Ni and b) ER/PDMS30/Ni particles systems. Coating thickness (t) is in μm. The horizontal line shows the onset of percolation [66].

The second simulation (Figure 4b) was performed for a system with 30 vol.% of PDMS. Figure 4b depicts the concentration of Ni in the ER on the x-axis (volume of PDMS is subtracted for comparability with Figure 4a). For the coating 1.95 μm is EPT reached again at 7.9 vol.% Ni in ER, i.e., 5.5 vol.% Ni in the composite system ER/PDMS30/Ni. This means that the percolation behaviour of the model does not depend on the addition of PDMS, which is in an agreement with expectations because the model does not reckon any irregularities in the localization of the filler like the concentration of conductive particles near the ER/PDMS interphase. However, the actual percolation of the ER/PDMS30/Ni system is 3.7 vol.% of Ni, which corresponds to 5.3 vol.% Ni in the ER (after deducting the volume of PDMS). This difference is due to the difference between the simulation, which contains a random independent

localization of particles in RVE, and the experiment with the preferential position of Ni particles near the PDMS surface observed, which significantly affects the final EPT.

4.2.3 Percolation threshold

Figure 5 shows the dependence of DC conductivity against conductive filler content measured at laboratory temperature for ER/PDMS/Ni composites. Both, ER and ER/PDMS blend are electrical insulators with very low values of conductivity $\sigma_{DC} \sim 10^{-12}$ S/cm. Polymer composites exhibit non-conductive behaviour with $\sigma_{DC} \sim (10^{-12}$–$10^{-9})$ S/cm at low filler concentrations up to the point where conductivity suddenly soars signifying the EPT with a simultaneous change of material character to conductor-like with the conductivity $\sigma_{DC} \sim (10^{-4}$–$10^{-2})$ S/cm. It is clearly visible that higher content of PDMS leads to a decrease in the critical percolation concentration. The polymer composites containing 0, 10, 20 and 30 vol.% of PDMS percolate at 7.9, 7.5, 4.6 and 3.7 vol.% of Ni, respectively. EPT of multiphase polymer composites are in good agreement with SEM images showing that Ni particles are excluded from the PDMS phase (Figure 3).
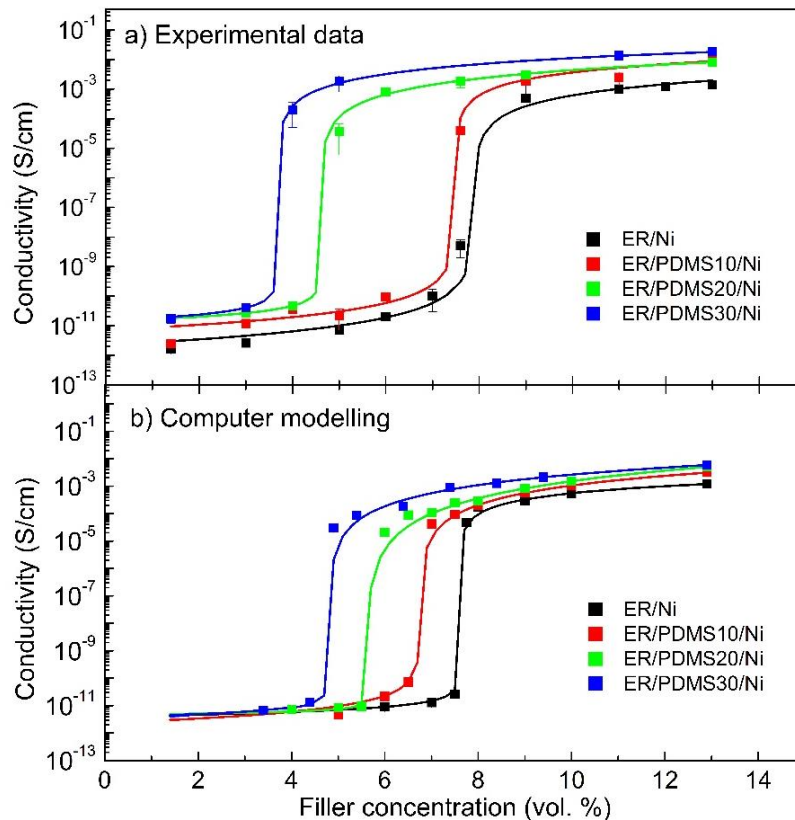

Figure 5: The concentration dependence of DC conductivities of a) prepared, b) simulated Ni [66].

Interestingly, values of the fitting *s* coefficient experimentally obtained (Eq. (1)) significantly differ among composites. It reaches approximately the value ≈ 1.4 for

systems without PDMS and with 10 vol.% of PDMS; however, systems with 20 and 30 vol.% of PDMS reach only a value of ≈ 0.6, similarly to fitting coefficients obtained by modelling. Nan et al. [70] state that s parameters should be in the range of 0.7–1; however, Dang et al. [71] also present a value of 1.4 for PVDF/Ni composites. Fitting coefficients above the percolation threshold (Eq. (2)) were calculated in the range $t ≈ 1$–2, which is in good agreement with both, theoretical predictions [3] and experimental results [72, 73].

4.2.4   Mechanical properties

Conductive composites based on the matrixes containing neat epoxy resin and polymer blend ER/PDMS30 were selected for mechanical testing. To evaluate mechanical properties, specimens ER/Ni8 and ER/PDMS30/Ni4 were prepared and tested for impact strength and lap shear strength and compare with pure ER and ER/PDMS30. It was found that the effect of Ni is negligible on impact strength; however, the addition of 30% of PDMS leads to an increase of impact strength by 60%. The results of lap shear strength show that the addition of both PDMS and Ni increases the adhesion of the material by ≈ 20%.

4.3 Ni-PANI particles

4.3.1   Chemistry of preparation/Synthesis

One of the most important conducting and electroactive polymers, PANI is prepared by oxidation of aniline hydrochloride with ammonium peroxydisulfate (Figure 6).
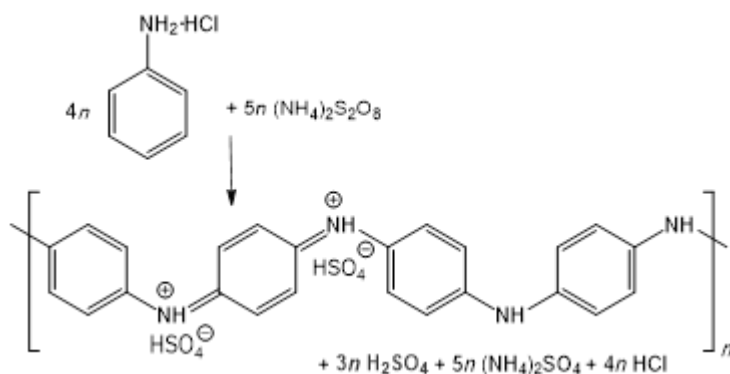

Figure 6: Aniline hydrochloride is oxidized with ammonium peroxydisulfate to PANI salt. Sulfuric acid is one of the by-products [67].

The preparation of neat PANI had a yield (107%) higher than the theoretical (considering only PANI) due to the presence of chloride, sulfate or hydrogen sulfate counterions. However, in the presence of Ni, the yield dropped to approximately 80% of the expectation (PANI + Ni). Considering the results of further analysis, the following scenario is probable: The starting reaction mixture contains aniline hydrochloride, ammonium peroxydisulfate (Figure 6). The hydrochloric acid present in this mixture does not dissolve nickel, even in the presence of peroxydisulfate. As the conversion from aniline to polyaniline

proceeds, sulfuric acid is produced as a by-product. This manifests itself in the drop of pH [39]. In the contrast to hydrochloric acid, dilute sulfuric acid dissolves nickel [74]. If Ni is present in the reaction mixture, the generated sulfuric acid reacts with Ni at the simultaneous evolution of hydrogen gas, $Ni + H_2SO_4 \rightarrow H_2(g) + NiSO_4$, as indeed observed at the end of the experiment.

Different amounts of Ni were used in the reaction mixture leading to different Ni concentrations in Ni-PANI mixture. There is a difference between theoretical Ni content with actual Ni content determined by TGA. For theoretical concentrations of Ni 18.7, 48.0 and 64.8 wt.%, the actual concentrations were 7.2, 40.2 and 58.8 wt.% which shows partial dissolution of Ni.

4.3.2 Morphology

Ni microparticles used in the experiments had the size of the units of micrometres with irregular hedgehog shape (Figure 7a). Figure 7b shows the morphology of Ni-PANI (19.9 wt.%) composite. It should be noted that the volume fraction of Ni is much lower due to the large difference between Ni and PANI densities 8.9 and 1.4 g/cm^3, respectively. For that reason, only dominating voluminous globular PANI coating is visible on the micrograph. The coating of the Ni microparticles with PANI is also demonstrated by transmission electron microscopy (Figure 8). Some free PANI accompanies them.
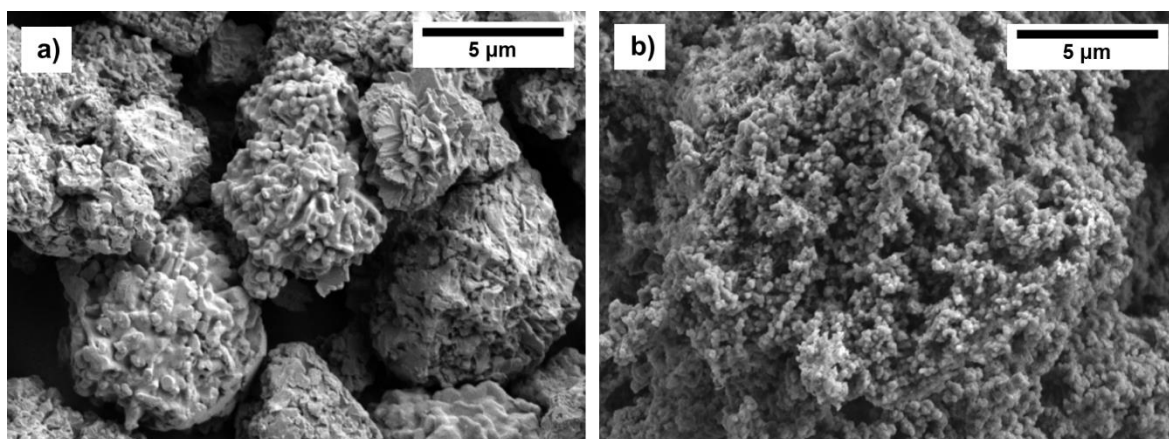

Figure 7: SEM micrograph of Ni microparticles (a) before and (b) after the coating with PANI [67].
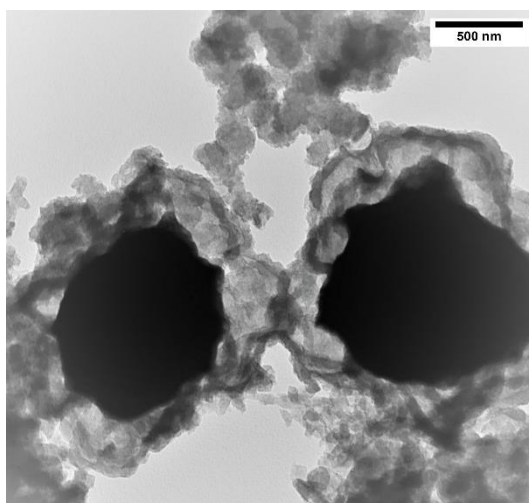
Figure 8: TEM micrograph of Ni-PANI (19.9 wt.%) core-shell particles [67].

4.3.3 Electrical conductivity

The resistivity of Ni-PANI powders measured as a function of pressure is in all cases lower than the conductivity of both components, PANI and Ni (Figure 9), but still at the level, which is satisfactory for various applications based on electrical properties. The spectroscopic analysis and EDAX suggest that this is due to the reduced degree of protonation of PANI. The resistivity decrease (i.e., the conductivity increase) by one up to two orders of magnitude can be achieved by the compression (Figure 9).

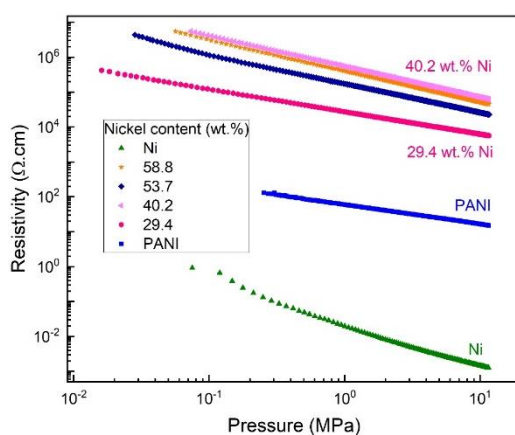*Figure 9: The dependence of the resistivity of Ni-PANI on applied pressure [67].*

4.4 TPU/Ni-PANI composites

4.4.1 Mechanical properties

For practical applications, illustrated below by the electromagnetic interference shielding, the Ni-PANI hybrids have to be converted to materials with suitable mechanical properties. For that reason, the hybrid powders were dispersed in a matrix of thermoplastic polyurethane.

The matrix exhibits a typical elastomeric behaviour with a relatively low Young modulus and tensile strength but excellent elongation in the order of hundreds of percent. The addition of PANI (0) or Ni-PANI fillers leads to the stiffening of the material while lowering elongation and maximum tensile strength. The limited interfacial interaction between neat Ni (100) particles and matrix brings back the elastomeric behaviour of composite; however, reduced in the comparison with TPU because the Ni particles act as defects stimulating the break at lower tensile strengths.

4.4.2 Electromagnetic interference shielding

Figure 10 shows the dependence of RAT contributions on Ni content in composite materials at the same 60 wt.% filler content. This means that as the Ni content increases, the content of PANI increases accordingly. The composite based exclusively on PANI had low transmission, $\approx 3\%$. The composite containing neat Ni reflects and absorbs about 60 and 20% of radiation, respectively, and about 20% of the electromagnetic energy wave is transmitted.
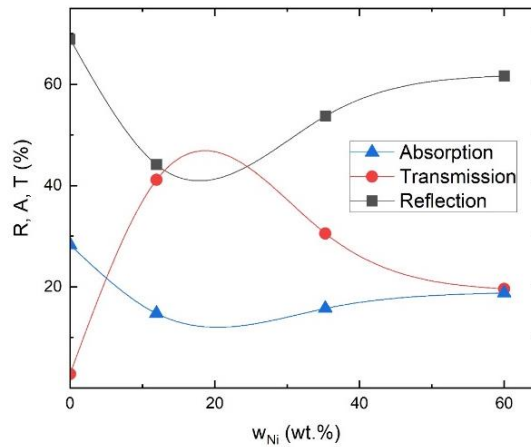

Figure 10: RAT contributions to the electromagnetic interference shielding at 9 GHz in dependence on Ni content in the composite with 60 wt.% Ni-PANI fillers [67].

It might be expected that the combination of PANI and Ni would lead to properties similar to these fillers, however, their transmission reached $\approx 40\%$ (Figure 10). This trend copies the conductivity pattern of Ni-PANI hybrids that have the conductivity lower than any of their constituents. This is caused by the presence of partly reduced PANI with an excess of non-conducting quinonedimine units, which does not contribute to shielding. Hence the reflection and absorption of the composites are mostly given by the Ni content. But still, less than 50% energy of the electromagnetic wave was transmitted through such a composite at 2 mm sample thickness.

4.5 MS/PPy/Fe$_3$O$_4$ structures

4.5.1 Chemistry of preparation/Synthesis

One of the most important conducting and electroactive polymers, PPy is prepared by the oxidation of pyrrole by iron(III) chloride (Figure 11).
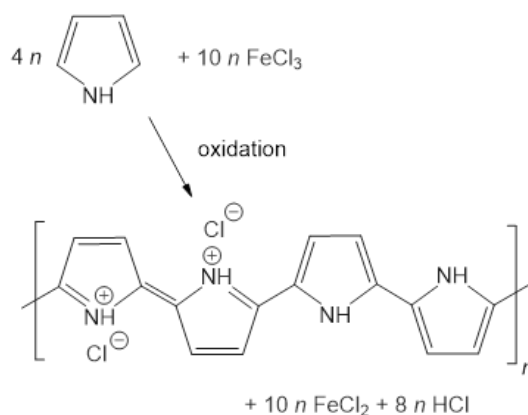

Figure 11: Pyrrole converts to PPy by oxidation with iron(III) chloride, iron(II) chloride is a by-product [21].

Magnetite (Fe$_3$O$_4$) was prepared by the chemical co-precipitation method based on the treatment of the mixture of iron(III) and iron(II) chlorides with aqueous ammonium hydroxide as a precipitant [53]:

$$2 \, FeCl_3 + FeCl_2 + 8 \, NH_4OH \rightarrow Fe_3O_4 + 4 \, H_2O + 8 \, NH_4Cl \qquad (10)$$

The obvious strategy how to produce the conducting and magnetic PPy/Fe$_3$O$_4$ mixture of particles is to use stoichiometric excess of iron(III) chloride in the preparation of PPy followed by the conversion of the resulting mixture of iron oxides to Fe$_3$O$_4$ by treatment with ammonia. This makes the composite preparation simple and convenient.

When the composite preparation is carried out in the presence of a melamine sponge (MS), the sponge becomes coated firstly with PPy and Fe$_3$O$_4$ precipitates after the subsequent treatment with ammonia. The content of PPy in the composite with MS was 21.1 wt.% as determined from the mass increase after polymer deposition. After the generation of Fe$_3$O$_4$ inside MS/PPy, the content of the inorganic part represented by iron oxides, 14.1 wt.%, was determined as ash. The content of PPy in this ternary composite was thus reduced to 18.1 wt.%.

4.5.2 Morphology

The coating of MS with a black PPy is well visible by SEM (Figure 12). The macroporous structure of the sponge is preserved and PPy is deposited on melamine as a thin polymer film with some adhering PPy nanoparticles. In the next step, Fe$_3$O$_4$ deposits as clusters of nanoparticles onto PPy coating. The open-pore structure of MS/PPy/Fe$_3$O$_4$ is maintained and macropores are not blocked by Fe$_3$O$_4$.
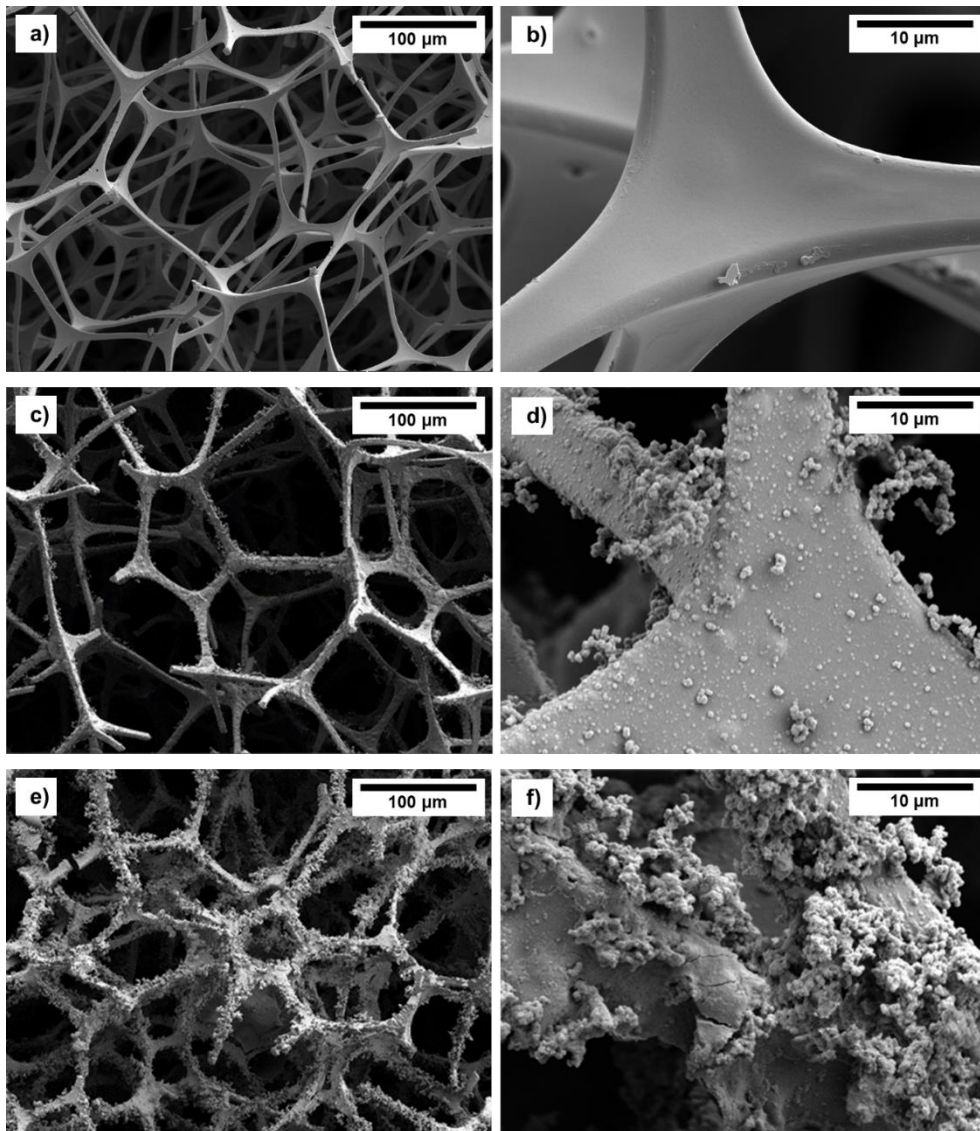
Figure 12: a, b) MS, c, d) MS/PPy, and e, f) MS/PPy/Fe₃O₄. Lower magnification (left) and higher (right) [21].

PPy has a typical morphology of fused globules, which become coated with Fe_3O_4 after subsequent treatment by ammonia. The presence of Fe_3O_4 becomes obvious as the composite becomes attracted to the magnet.

4.5.3   Electrical conductivity

Insulative MS changes to a conductor (0.05 S/cm) after the deposition of PPy layer, which further increases during the compression to the maximum (0.23 S/cm). This is close to the conductivity of neat globular PPy, which is close to 1 S/cm [75, 76, 77].

Conducting PPy is deposited in the individual threads of the sponge (Figure 12) and the conducting pathways are thus created. During the continuing compression, the number of pathways within the infinitesimal cross-section will increase and conductivity will do so accordingly (Figure 13). At high compression; however,

some threads are expected to break thus reducing the number of pathways and, consequently, also the conductivity.

After the deposition of Fe_3O_4, the conductivity decreased only moderately to 0.021 S/cm (Figure 13). The decrease to a partial deprotonation of PPy under alkaline conditions is used for the generation of Fe_3O_4, which is associated with a decrease in conductivity [78].
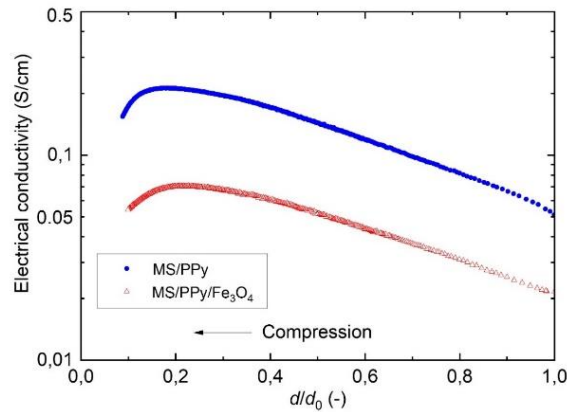

Figure 13: Electrical conductivity as a function of compression, i.e., the reduction of the relative height of cylindrical sample d/d_0. The starting height $d_0 \approx 8$ mm [21].

4.5.4 Electromagnetic Radiation Shielding

The experimental data describing the sponges (thickness 20 mm) are little dependent on the radiation frequency (Figure 14a). On a relative basis, they can be presented as the analysis of the individual contributions to the shielding, which are, consequently, qualitatively similar for the individual frequencies (Figure 14b).
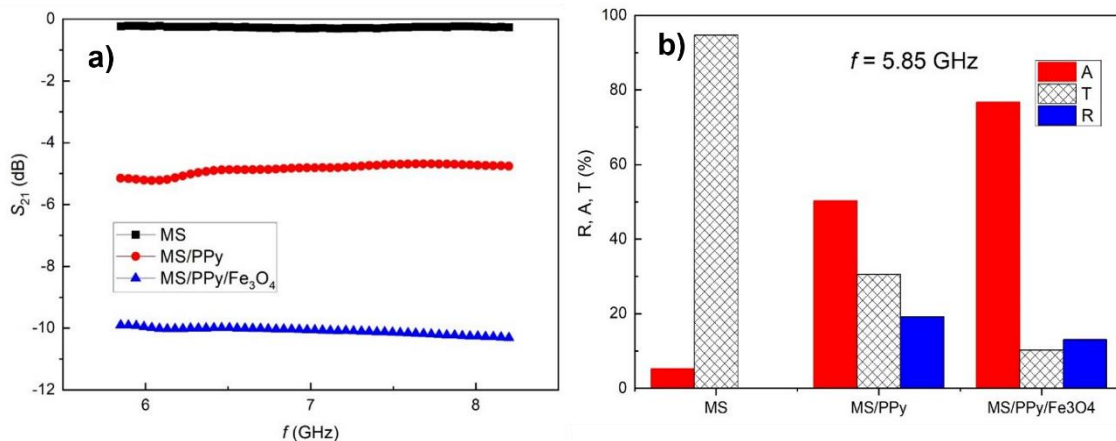
Figure 14: Frequency dependence of a) reverse transmission coefficient S_{21} and b) RAT contributions to the electromagnetic interference shielding at 5.85 GHz [21].

For the original MS, there is practically no radiation absorption and reflection (Figure 14b) at frequency 5.85 GHz. PPy coating introduces a marked increase in reflection ($\approx 20\%$), as might be expected from the conducting material; however, even higher increase was observed in absorption ($\approx 50\%$). Fe_3O_4 is generated under

the alkaline condition where PPy salt converts to PPy base, and the conductivity is reduced [78] and the reflectance decreases accordingly ($\approx$ 15%). The presence of Fe_3O_4 in the structure clearly adds to the absorption ($\approx$ 75%). The combination of the electrically conducting and magnetic components is thus beneficial for the shielding efficiency, and the transmission substantially decreases ($\approx$ 10%).

4.6 PPy coated melamine sponges

4.6.1 Carbonization

The carbonization of PPy powders was studied in detail for various morphologies, such as globular PPy and PPy nanofibers and nanotubes [62]. The process had three distinct phases. (1) Conducting PPy salts became deprotonated (250 °C) to PPy [78], (2) degradation of polymer chains (400 °C) with associated loss of conductivity and (3) conductivity recovery at a still higher temperature in response to continuing carbonization. It was assumed that a similar scenario would also be applicable to PPy composites, here PPy deposited on melamine sponges (MS), which is considered in the subsequent discussion.

4.6.2 Morphology

After the polymerization of pyrrole, the threads in the melamine sponge became coated with a compact PPy film with some adhering PPy globules and their clusters (Figure 15a,b).
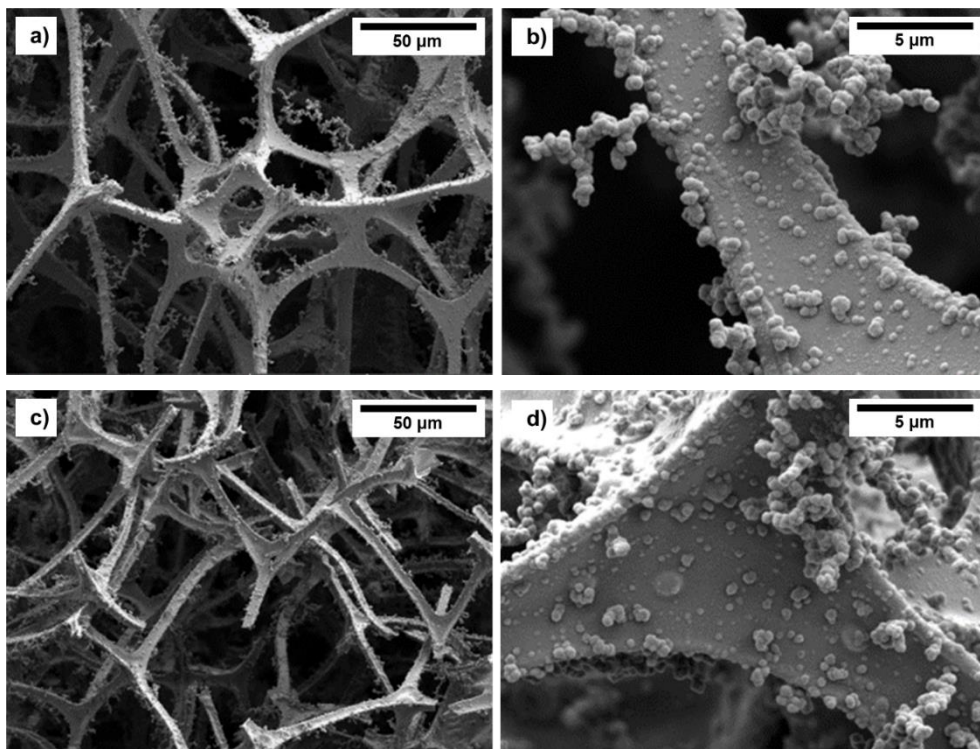

Figure 15: SEM micrographs of MS/PPy structures: a, b) before, and c, d) after carbonization at 650 °C taken at lower (left) and higher magnification (right) [68].

31

Based on previous studies comparing the uncoated and PPy-coated sponges (Figure 12), the PPy shell was estimated to be of a submicrometre thickness [79]. It had already been established that the morphology did not change after carbonization (Figure 15c,d) [61], except for a small shrinkage observable only on macroscopic samples.

4.6.3 Electrical conductivity

The resistivity was determined by the four-point van der Pauw method during compression from a pressure of approximately 0.01 up to 1 MPa. In the double-logarithmic presentation, when resistivity is plotted against sample thickness, the curves are close to straight lines with approximately the same slope (Figure 16a).

When the results are plotted in terms of the conductivity determined at fixed 0.1 MPa pressure (Figure 16b), a drop in the conductivity due to PPy deprotonation was observed [78] followed by decomposition at close to 400 °C, and then by recovery of conductivity due to carbonization in the course of temperature increase to 700 °C. Based on the above spectroscopic analysis of molecular structure, the following explanation is suggested: During the deprotonation associated with the loss of hydrochloric acid, the number of charge carriers represented by cation radicals (polarons) on PPy chains becomes reduced. The chain conjugation, i.e., the alternation of single and double bonds in PPy, is damaged and, consequently, conducting pathways are broken. Both effects result in the decrease of conductivity at 400 °C. The conjugated structure recovers during the graphitization by the generation of new double bonds at higher carbonization temperature with the consequent increase in the conductivity.
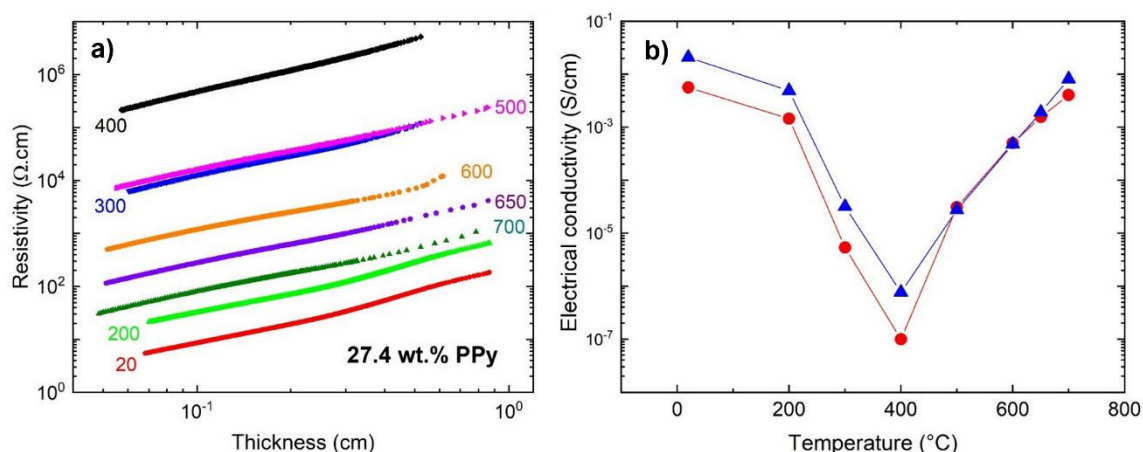

Figure 16: a) Dependance of resistivity of MS/PPy exposed to various temperatures 20–700 °C on the sample thickness during compression at 0.04–1 MPa pressure. b) Electrical conductivity of the MS/PPy exposed to various temperatures determined at 0.1 MPa pressure [68].

4.6.4   Electromagnetic Radiation Shielding

The radiation shielding of MS/PPy was practically independent of frequency in the range 8.2–12.4 GHz (Figure 17a). For that reason, only the data obtained at 9 GHz are reported below.

By comparing the shielding contributions (Figure 17b) with the electrical conductivity (Figure 16b), the qualitative correlation between these quantities is obvious. This applies especially to the radiation absorption. It decreased to zero as the carbonization temperature reached 400–500 °C and the conductivity dropped. However, the absorption of radiation recovered at higher carbonization temperatures in accordance with the increase in electrical conductivity. The radiation reflection followed the same pattern, but its contribution was significantly lower than that of the absorption.
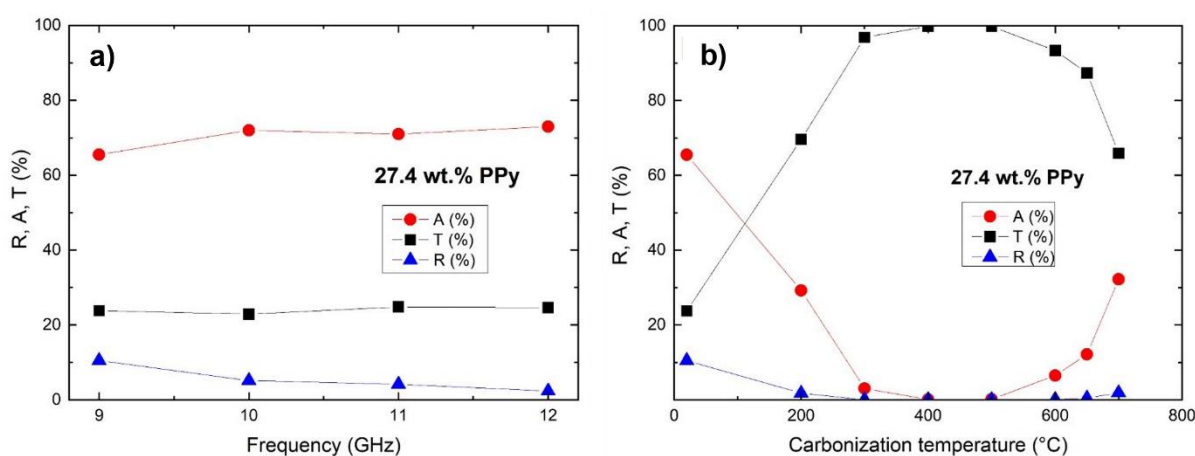
Figure 17: a) Frequency dependance and b) carbonization temperature dependance of RAT contributions to the electromagnetic interference shielding for MS/PPy containing 27.4 wt.% PPy [68].

The conductivity; however, is not the sole parameter that controls shielding efficiency. Changes in the molecular structure and surface properties occurring during carbonization are also likely to affect, for instance, multiple internal reflections, and thus contribute to radiation shielding.

5. CONCLUSIONS

The electric properties of two-phase polymer blends (ER and PDMS) filled with conductive Ni particles with the hedgehog-like structure were investigated experimentally and by computational modelling. The multi-phase composites exhibited reduced percolation thresholds and enhanced conductivities above that of the individually Ni-filled ER.

It is crucial that conductive Ni particles are selectively located not only in the continuous ER phase but preferentially in the interphase of ER/PDMS as was observed on SEM micrographs. The percolation threshold of the ER/PDMS/Ni composites was reached at 3.7 vol.% Ni particles, where the DC conductivity rose by 7 orders of magnitude. This EPT of the polymer blend was reached at a significantly lower Ni content and thereby weight than the individually filled ER (7.9 vol.%). It leads to a decrease not only in the density from 1.7 g/cm^3 to 1.4 g/cm^3 but also in the cost of the final composite product.

Prior to the actual preparation of polymer composites, the system was simulated using the three-dimensional Monte Carlo model. It was found, that at low PDMS concentrations, the simulations were quite precise in comparison with measured data of DC conductivity. However, the results of the simulations at higher concentrations of PDMS underestimated the value of the percolation threshold, which in the ER/PDMS30/Ni system was found to be 3.7 vol.%, instead of 4.9 vol.% reached in simulation due to different filler localization.

The mechanical properties of conductive Ni-based composite adhesives were tested by the lap shear test. The composites containing 30 vol.% of PDMS exhibit better adhesion (by 20%) to the metal plates than neat epoxy resin. The impact strength of composite materials was tested by the Charpy impact test. The inclusion of PDMS in ER enhanced impact strength by 75%.

<p style="text-align:center">***</p>

Ni-PANI core-shell particles were prepared by the oxidation of aniline hydrochloride with ammonium peroxydisulfate in an aqueous medium containing nickel microparticles. As the oxidation proceeded, sulfuric acid had been generated as a by-product. In contrast to hydrochloric acid, which does not dissolve Ni, sulfuric acid does. This resulted in the partial dissolution of Ni and thus a decrease in the size of particles which might be beneficial for some applications.

Synthesized particles were characterized by spectroscopy techniques and their electromagnetic properties were studied. However, the results suggested that hydrogen gas generated during the dissolution caused partial hydrogenation of PANI which was catalysed by Ni. This reduced the degree of protonation in polyaniline and led to the decrease in the conductivity of core-shell particles

to 10^{-3}–10^{-2} S/cm, i.e., below the conductivity of polyaniline alone, ~ 1 S/cm, and nickel powder ~ 1,000 S/cm.

Polymer composites based on thermoplastic polyurethane filled with 60 wt.% of Ni-PANI core-shell particles were prepared. The mechanical properties of TPU/Ni-PANI composites were tested by the tensile test. The addition of neat PANI or Ni-PANI particles leads to significant stiffening of the composite (2 orders of magnitude) while lowering elongation and maximum tensile strength. This is the result of the blending TPU matrix and PANI. The addition of neat Ni particles brings back the elastomeric behaviour of composite with higher stiffness but lower tensile strengths compared with TPU.

TPU/Ni-PANI composites were further tested for shielding efficiency at 9 GHz for 2 mm sample thickness. The composites were able to absorb and reflect more than 50% of the energy of the incident electromagnetic wave. It should be noted; however, that those based on individual components were even more efficient, thus reducing the transmission below 20% and 3% for Ni and PANI alone dispersed in a polyurethane matrix.

<p style="text-align:center">***</p>

Polypyrrole was deposited in situ on the macroporous open-cell melamine sponge (MS) by the oxidation of pyrrole with iron(III) chloride in stoichiometric excess. After finishing polymerization, the usage of magnetite co-precipitation was initiated by treatment with an ammonia solution. The conducting MS/PPy produced in the first step is thus coated by Fe_3O_4 particles. The purity of the product was determined by ATR FTIR spectroscopy and elemental analysis.

The dependence of electrical conductivity on the sponge compression and also magnetic properties were determined. Although the MS/PPy/Fe_3O_4 ferrosponge exhibit slightly lower conductivity (0.02 S/cm) than MS/PPy (0.05 S/cm), it is compensated by two orders of magnitude higher magnetisation $M_s = 12.3$ emu/g. The measurement of electromagnetic shielding in microwave radiation proved that the addition of magnetisation is crucial for good shielding properties. While the measured transmission of MS/PPy was $\approx$ 30%, it was only $\approx$ 10% for MS/PPy/Fe_3O_4. This can be attributed to higher absorption which increased from $\approx$ 50% to $\approx$ 75%.

<p style="text-align:center">***</p>

MS/PPy macroporous open-cell structures were carbonized by exposition to various temperatures up to 700 °C in an inert atmosphere. The macroporous structure and mechanical integrity were preserved after this process. This converted both the PPy and the MS to a macroporous nitrogen-containing carbon structure. The carbon content increased from 40 to 65 wt.% after carbonization, while nitrogen content dropped from 40 wt.% to still reasonable 20 wt.%. The porosity of the material approximately quadrupled during the carbonization,

<p style="text-align:center">35</p>

measured by both specific surface area (an increase from 70 to 300 m^2/g) and pores volume (an increase from 0.07 to 0.25 cm^3/g). Changes in the molecular structure during the carbonization were determined by elemental analysis and ATR FTIR.

The electrical conductivity of the MS/PPy was measured as a function of compression. The conductivity of the original MS/PPy containing 27.4 wt.% of pyrrole $\approx$ 0.2 S/cm was reduced by five orders of magnitude when exposed to 400 °C and recovered to $\approx$ 0.03 S/cm after the temperature reached 700 °C. Carbonization temperature dependence of electromagnetic microwave absorbance of MS/PPy structures followed a similar trend. Firstly, absorption drops at temperatures around 400 °C, but it increases afterwards with further carbonization.

CONTRIBUTION TO SCIENCE

The first part of this work, focusing on conductive polymer composites, brings together a unique combination of experimental science and computer simulation for a multi-component system based on immiscible polymer blends. The authors have been unable to find any other study that deals with computer modelling of an immiscible polymer blend with a conductive filler or a polymer composite with two fillers one of which is conductive and the other is non-conductive. Let alone a study combining such a simulation with an experiment. Moreover, two quite different approaches, based on the Monte Carlo method, have been shown to simulate percolation in a multicomponent system. This, according to the authors, is a greater contribution to science than the developed procedure for reaction mixing of ER and PDMS or the excellent results achieved by the presented material in electrical and mechanical tests.

In the second part of this work, which focused on the preparation of Ni-PANI core-shell particles, interesting results were obtained. Probably the greatest contribution is the description of the complex chemical reactions taking place during the polymerization of PANI in the presence of Ni. Although Ni does not react with the reactants used in the reaction, one of the by-products was found to be able to dissolve Ni. This in itself could be useful as it would allow the preparation of different particle sizes from one type of material depending on the initial conditions. Unfortunately, it was found that the hydrogen released by this reaction is catalyzed by Ni and partially hydrogenates PANI, leading to a decrease in conductivity.

The third part of this work focuses on the coating of porous organic structures. The main contribution of this work is the subsequent functionalization of these structures for improved properties. One way was to use the by-products of PPy polymerization to coprecipitate magnetic Fe_3O_4 particles. In this way, ferrosponges were formed, which is a relatively new concept. The ferrosponges prepared so far have been based on hydrogels and not on cheap commercially available porous material. The authors were also unable to find any study where the prepared ferrosponges were electrically conductive. This led to good results in the area of electromagnetic shielding. Another way to functionalize these structures was carbonization, which resulted in a large increase in porosity and a decrease in mass while maintaining electrical conductivity.

REFERENCES

[1]   KIMURA, Toyoaki et al. Self-temperature-control plane heaters by polyethylene glycol-graphite systems. *3. Polymer*. 1996, 37(14), 2981-87. doi: 10.1016/0032-3861(96)89395-5.

[2]   MUSINO, Dafne et al. Structural identification of percolation of nanoparticles. *Nanoscale*. 2020, 12, 3907-15. doi: 10.1039/C9NR09395H.

[3]   KIRKPATRICK, Scott. Percolation and Conduction. *Reviews of Modern Physics*. 1973, 45(4), 574-588. doi: 10.1103/RevModPhys.45.574.

[4]   BALBERG, I. et al. Percolation Thresholds in the Three-Dimensional Sticks System. *Physical Review Letters*. 1984, 52(17), 1465-68. doi: 10.1103/PhysRevLett.52.1465.

[5]   WU, Guozhang et al. A Self-Assembled Electric Conductive Network in Short Carbon Fiber Filled Poly(methyl methacrylate) Composites with Selective Adsorption of Polyethylene. *Macromolecules*. 1999, 32(10), 3534-36. doi: 10.1021/ma981806a.

[6]   FOULGER, Stephen H. Electrical Properties of Composites in the Vicinity of the Percolation Threshold. *Journal of Applied Polymer Science*. 1999, 72(12), 1573-82. doi: 10.1002/(SICI)1097-4628(19990620)72:12<1573::AID-APP10>3.0.CO;2-6.

[7]   FOULGER, Stephen H. Reduced percolation thresholds of immiscible conductive blends. Journal of *Polymer Science Part B: Polymer Physics*. 1999, 37(15), 1899-1910. doi: 10.1002/(sici)1099-0488(19990801)37:153.0.co;2-0.

[8]   VILČÁKOVÁ, Jarmila et al. Effect of Surfactants and manufacturing methods on the electrical and thermal conductivity of carbon nanotube/silicone composites. *Molecules*. 2012, 17(11), 13157-74. doi: 10.3390/molecules171113157.

[9]   SAGALIANOV, Igor et al. Synergistic Enhancement of the Percolation Threshold in Hybrid Polymeric Nanocomposites Based on Carbon Nanotubes and Graphite Nanoplatelets. *Nanoscale Research Letters*. 2014, 12, 140-146. doi: 10.1186/s11671-017-1909-z.

[10]   MANTESE, Joseph V. et al. Applicability of effective medium theory to ferroelectric/ferrimagnetic composites with composition and frequency-dependent complex permittivities and permeabilities. *Journal of Applied Physics*. 1996, 79, 1655-1660. doi: 10.1063/1.361010.

[11]   SCHER, Harvey and ZALLEN, Richard. Critical Density in Percolation Processes. *The Journal of Chemical Physics*. 1970, 53, 3759-61. doi: 10.1063/1.1674565.

[12]   GAO, Cong et al. High-performance conductive materials based on the selective location of carbon black in poly(ether ether ketone)/polyimide matrix. *Composites Part B: Engineering*. 2015, 79, 124-131. doi: 10.1016/j.compositesb.2015.03.047.

[13]   IBARRA-GÓMEZ, Rigoberto et al. Influence of the Blend Viscosity and Interface Energies on the Preferential Location of CB and Conductivity of BR/EPDM Blends. *Rubber Chemistry and Technology*. 2003, 76(4), 969-978. doi: 10.5254/1.3547785.

[14]   HUANG, Ying et al. Effects of the filler size on the electrical percolation threshold of carbon black-carbon nanotube-polymer composites. *Journal of Applied Polymer Science*. 2018, 135(32), 1-8. doi: 10.1002/app.46517.

[15]   DALMAS, Florent et al. Carbon nanotube-filled polymer composites. Numerical simulation of electrical conductivity in three-dimensional entangled fibrous networks. *Acta Materialia*. 2006, 54(11), 2923-31. doi: 10.1016/j.actamat.2006.02.028.

[16]   XIONG, Zhuo-Yue et al. Modeling the electrical percolation of mixed carbon fillers in polymer blends. *Carbon*. 2014, 70, 233-240. doi: 10.1016/j.carbon.2014.01.001.

[17]   GÖLDEL, Andreas et al. Shape-Dependent Localization of Carbon Nanotubes and Carbon Black in an Immiscible Polymer Blend during Melt Mixing. *Macromolecules*. 2011, 44(15), 6094–6102. doi: 10.1021/ma200793a.

[18]   AL-SALEH, Mohamed H. Clay/carbon nanotube hybrid mixture to reduce the electrical percolation threshold of polymer nanocomposites. *Composites Science and Technology*. 2017, 149, 34-40. doi: 10.1016/j.compscitech.2017.06.009.

[19]   FENG, Xuebin et al. Electrical Conductivity and Microwave Absorbing Properties of Nickel-Coated Multiwalled Carbon Nanotubes/Poly(phthalazinone ether sulfone ketone)s Composites. *Polymer Engineering and Science*. 2008, 48(5), 1007-1014. doi: 10.1002/pen.21028.

[20]   STEJSKAL, Jaroslav. Conducting polymers are not just conducting: a perspective for emerging technology. *Polymer International*. 2020, 69(8), 662–664. doi: 10.1002/pi.5947.

[21]   STEJSKAL, Jaroslav et al. One-pot preparation of conducting melamine/polypyrrole/magnetite ferrosponge. *ACS Applied Polymer Materials*. 2021, 3(2), 1107–1115. doi: 10.1021/acsapm.0c01331.

[22]   CHUNG, D. D. L. Materials for electromagnetic interference shielding. *Materials Chemistry and Physics*. 2000, 255(9), 350–354. doi: 10.1016/j.matchemphys.2020.123587.

[23]   KUMA, Rajeev et al. Lightweight carbon-red mud hybrid foam toward fire-resistant and efficient shield against electromagnetic interference. *Scientific Reports*. 2020, 10(1), 9913. doi: 10.1038/s41598-020-66929-3.

[24]   SULTAN, J. N. and MCGARRY, F. J. Effect of rubber particle size on deformation mechanisms in glassy epoxy. *Polymer Engineering & Science*. 1973, 13(1), 29-34. doi: 10.1002/pen.760130105.

[25]   CALDONA, Eugene B. et al. A Review on Rubber-Enhanced Polymeric Materials. *Polymer Reviews*. 2017, 57(2), 311-338. doi: 10.1080/15583724.2016.1247102.

[26]   OZTURK, A. et al. Effects of liquid rubber modification on the behaviour of epoxy resin. *European Polymer Journal*. 2001, 37(12), 2353-63. doi: 10.1016/S0014-3057(01)00158-6.

[27]   IMANAKA, Makoto et al. Crack-growth behavior of epoxy adhesives modified with liquid rubber and cross-linked rubber particles under mode I loading. *International Journal of Adhesion and Adhesives*. 2009, 29(1), 45-55. doi: 10.1016/j.ijadhadh.2007.11.004.

[28]   SPRENGER, Stephan. Fiber-reinforced composites based on epoxy resins modified with elastomers and surface-modified silica nanoparticles. *Journal of Materials Science*. 2014, 49(6), 2391-2402. doi: 10.1007/s10853-013-7963-8.

[29]   WANG, Lian et al. Investigations on the Morphologies and Properties of Epoxy/acrylic Rubber/nanoclay Nanocomposites for Adhesive Films. *Composites Science and Technology*. 2014, 93(1), 46-53. doi:doi.org/10.1016/j.compscitech.2013.12.023.

[30]   VIJU, Susan Mathew et al. High Performance HTLNR/epoxy Blend-Phase Morphology and Thermo-Mechanical Properties. *Journal of Applied Polymer Science*. 2012, 125(1), 804-811. doi: 10.1002/app.35446.

[31]   DEHAGHI, Hamidreza Ali-Asgari et al. Thermal and Morphological Characteristics of Solution Blended epoxy/NBR Compound. *Journal of Thermal Analysis and Calorimetry*. 2013, 114(1), 185-94. doi: 10.1007/s10973-012-2920-3.

[32]   PARK, Soo-Jin et al. Synthesis of a Novel Siloxane-Containing Diamine for Increasing Flexibility of Epoxy Resins. *Materials Science and Engineering: A*. 2005, 399(1-2), 377-381. doi: 10.1016/j.msea.2005.04.020.

[33]   MIWA, Minoru et al. Volume Fraction and Temperature Dependence of Mechanical Properties of Silicone Rubber Particulate/epoxy Blends. *Composites*. 1995, 26(5), 371-377. doi: 10.1016/S0010-4361(06)80136-9.

[34]   PARAMESWARANPILLAI, Jyotishkumar et al. Micro Phase Separated Epoxy/poly(ε-Caprolactone)-Block-Poly(dimethyl Siloxane)-Block-Poly(ε-caprolactone)/4,4′-Diaminodiphenylsulfone Systems: Morphology, Viscoelasticity, Thermo-Mechanical Properties and Surface Hydrophobicity. *Polymer Testing*. 2016, 55(8), 115-122. doi: 10.1016/j.polymertesting.2016.08.016.

[35]   WANG, Tao et al. Acrylate Copolymers as Impact Modifier for Epoxy Resin. *Journal Wuhan University of Technology - Materials Science Edition*. 2015, 30(6), 1210-14. doi: 10.1007/s11595-015-1297-0.

[36]   TRZEPIECIŃSKI, Thomasz et al. Modelling of multilayer actuator layers by homogenisation technique using Digimat software. *Ceramics International*. 2017, 43(3), 3259-66. doi: 10.1016/j.ceramint.2016.11.157.

[37]   MANTA, Asimina et al. Simulated electrical response of randomly distributed and aligned graphene/polymer nanocomposites. *Composite Structure*. 2018, 192, 452–459. doi: 10.1016/j.compstruct.2018.03.022.

[38]   NILSSON, Fritjof et al. Simulating the effective electric conductivity of polymer composites with high aspect ratio fillers. *Composites Science and Technology*. 2016, 132, 16-23. doi: 10.1016/j.compscitech.2016.06.008.

[39]   STEJSKAL, Jaroslav et al. *Conducting Polymers: Polyaniline*. In: Encyclopedia of Polymer Science and Technology, Wiley Online Library: Hoboken, NJ, USA, 2015; pp. 1–44. doi: 10.1002/0471440264.pst640.

[40]   DONG, Xing Long et al. Enhanced microwave absorption in Ni/polyaniline nanocomposites by dual dielectric relaxation. *Applied Physics Letters*. 2008, 92(1), 013127. doi: 10.1063/1.2830995.

[41]   MOON, Il Jae et al. Fabrication of dopamine grafted polyaniline/carbonyl iron core-shell typed microspheres and their magnetorheology. *Colloids and Surfaces A: Physicochemical and Engineering Aspects*. 2016, 500, 137–145. doi: 10.1016/j.colsurfa.2016.04.037.

[42]   TIAN, Xiaoli et al. Flower-like Fe2O3/polyaniline core/shell nanocomposite and its electrorheological properties. *Colloids and Surfaces A: Physicochemical and Engineering Aspects*. 2016, 498, 185–193. doi: 10.1016/j.colsurfa.2016.03.054.

[43]   CHOWDHURY, Al-Nakib et al. Polyaniline matrix containing nickel ferromagnet. *Journal of Applied Polymer Science*. 2005, 103(1), 321–327. doi: 10.1002/app.23958.

[44]   CHEN, Xingliang et al. Preparation and microwave absorbing properties of nickel-coated carbon fiber with polyaniline via in situ polymerization. *Journal of Materials Science: Materials in Electronics*. 2016, 27, 5607–5612. doi: 10.1007/s10854-016-4466-9.

[45]   GAO, Zhiyong et al. Catalytic electrode-redox electrolyte supercapacitor system with enhanced capacitive performance. *Chemical Engineering Journal*. 2018, 335, 590–599. doi: 10.1016/j.cej.2017.11.037.

[46]   HEINIG, Nina F. et al. The growth of nickel nanoparticles on conductive polymer composite electrodes. *Materials Letters*. 2008, 62(15), 2285–2288. doi: 10.1016/j.matlet.2007.11.094.

[47]   DAMIAN, Alexis and OMANOVIC, Sasha. Ni and Ni-Mo hydrogen evolution electrocatalysts electrodeposited in polyaniline matrix. *Journal of Power Sources*. 2006, 158(1), 464–476. doi: 10.1016/j.jpowsour.2005.09.007.

[48]   SHAH, Sayed Shaheen et al. Boosting the electrochemical performance of polyaniline by one-step electrochemical deposition on nickel foam for high-performance asymmetric supercapacitor. *Polymers*. 2022, 14(2), 270. doi: 10.3390/polym14020270.

[49]   STEJSKAL, Jaroslav. Interaction of conducting polymers, polyaniline and polypyrrole, with organic dyes: polymer morphology control, dye adsorption and photocatalytic decomposition. *Chemical Papers*. 2020, 74, 1–54. doi: 10.1007/s11696-019-00982-9.

[50] BHAUMIK, Madhumita et al. Metallic nickel nanoparticles supported polyaniline nanotubes as heterogeneous Fenton-like catalyst for the degradation of brilliant green dye in aqueous solution. *Journal of Colloid and Interface Science.* 2022, 611, 408–420. doi: 10.1016/j.jcis.2021.11.181.

[51] BHAUMIK, Madhumita et al. Zero valent nickel nanoparticles decorated polyaniline nanotubes for the efficient removal of Pb(II) from aqueous solution: synthesis, characterization and mechanism investigation. *Chemical Engineering Journal.* 2021, 417, 127910. doi: 10.1016/j.cej.2020.127910.

[52] GANGULY, Sayan and MARGEL, Shlomo. Review: Remotely controlled magneto-regulation of therapeutics from magnetoelastic gel matrices. *Biotechnology Advances.* 2020, 44, 107611. doi: 10.1016/j.biotechadv.2020.107611.

[53] GETIREN, Bengü et al. NIR-responsive Fe3O4@PPy nanocomposite for efficient potential use in photothermal therapy. *Journal of Applied Polymer Science.* 2020, 137(44), 49343. doi: 10.1002/app.49343.

[54] SHUKLA, Vineeta. Role of spin disorder in magnetic and EMI shielding properties of Fe3O4/C/PPy core/shell composites. *Journal of Materials Science.* 2020, 55(21), 2826–2835. doi: 10.1007/s10853-019-04198-w.

[55] TANG, Shun et al. Facile synthesis of Fe3O4@PPy core–shell magnetic nanoparticles and their enhanced dispersity and acid stability. *Materials & Design.* 2017, 121, 47–50. doi: 10.1016/j.matdes.2017.02.049.

[56] LI, Jinhuan et al. Three-dimensional graphene supported Fe3O4 coated by polypyrrole toward enhanced stability and microwave absorbing properties. *Journal of Materials Research and Technology.* 2020, 9(1), 762–772. doi: 10.1016/j.jmrt.2019.11.016.

[57] FENG, Yi and YAO, Jianfeng. Design of melamine sponge-based three-dimensional porous materials toward applications. *Industrial & Engineering Chemistry Research.* 2018, 57(22), 7322–7330. doi: 10.1021/acs.iecr.8b01232.

[58] CHEN, Shuiliang et al. Elastic carbon foam via direct carboni-zation of polymer foam for flexible electrodes and organic chemical absorption. *Energy & Environmental Science.* 2013, 6(8), 2435–2439. doi: 10.1039/c3ee41436a.

[59] JING, Xiangxia et al. Regulating capacitative perfor-mance of monolithic carbon sponges by balancing heteroatom content, surface area and graphitization degree. *ChemNanoMat.* 2020, 6(10), 1507–1512. doi: 10.1002/cnma.202000358.

[60] ISMAEL, Mohammed. A review on graphitic carbon nitride (g-C3N4) based nanocomposites: Synthesis, categories, and their application in photocatalysis. *Journal of Alloys and Compounds.* 2020, 846, 156446. doi: 10.1016/j.jallcom.2020.156446.

[61] ĆIRIĆ-MARJANOVIĆ, Gordana et al. Carbonised polyaniline and polypyrrole: Towards advanced nitrogen-containing carbon materials. *Chemical Papers.* 2013, 67, 781–813. doi: 10.2478/s11696-013-0312-1.

[62] STEJSKAL, Jaroslav et al. Conversion of conducting polypyrrole nanostructures to nitrogen-containing carbons and its impact on the adsorption of organic dye. *Materials Advances.* 2021, 2, 706–717. doi: 10.1039/d0ma00730g.

[63] KOPECKÁ, Jitka et al. Polypyrrole nanotubes and their carbonized analogs: Synthesis, characterization, gas sensing properties. *Sensors.* 2016, 16(11), 1917. doi: 10.3390/s16111917.

[64] VILČÁKOVÁ, Jarmila et al. Enhanced Charpy impact strength of epoxy resin modified with vinyl-terminated polydimethylsiloxane. *Journal of Applied Polymer Science.* 2018, 135(4), 1-12. doi: 10.1002/app.45720.

[65] JURČA, Marek. *The Development and Characterization of Epoxy-Silicone Blends as a Matrix for Antistatic Composites.* Zlín: Univerzita Tomáše Bati ve Zlíně, 2017, 100 s. Dostupné

také z: http://hdl.handle.net/10563/40737. Univerzita Tomáše Bati ve Zlíně. Fakulta technologická, Ústav inženýrství polymerů. Vedoucí práce Vilčáková, Jarmila.

[66]   JURČA, Marek et al. Reduced percolation threshold of conductive adhesive through nonuniform filler localization: Monte Carlo simulation and experimental study. *Composites Science and Technology*. 2021, 214, 108964. doi: 10.1016/j.compscitech.2021.108964.

[67]   JURČA, Marek et al. Conducting and magnetic hybrid polyaniline/nickel composites. *Synthetic Metals*. 2022, 291, 117165. doi: 10.1016/j.synthmet.2022.117165.

[68]   STEJSKAL, Jaroslav et al. Polypyrrole-Coated Melamine Sponge as a Precursor for Conducting Macroporous Nitrogen-Containing Carbons. *Coatings*. 2022, 12(3), 324. doi: 10.3390/coatings12030324.

[69]   PAUW, L. J. van der. A method of measuring specific resistivity and Hall effect of discs of arbitrary shape. *Semiconductor Devices: Pioneering Papers*. 1991, 13, 174-182. doi: 10.1142/9789814503464_0017.

[70]   NAN, Ce-Wen. Physics of inhomogeneous inorganic materials. *Progress in Materials Science*. 1993, 37(1), 1-116. doi: 10.1016/0079-6425(93)900045.

[71]   DANG, Zhi-Ming et al. Novel Ferroelectric Polymer Composites with High Dielectric Constants. *Advanced Materials*. 2003, 15(19), 1625-29. doi: 10.1002/adma.200304911.

[72]   MAMUNYA, E. P. et al. Percolation conductivity of polymer composites filled with dispersed conductive filler. *Polymer Composites*. 1995, 16(4), 319–24. doi: 10.1002/pc.750160409.

[73]   CLARKE, P. S. et al. Electrical-conductivity and Hall-effect measurements in semiconducting powders. Study of percolation effects. *Physical Review B*. 1978, 18(4), 1813–17. doi: 10.1103/PhysRevB.18.1813.

[74]   ITAGAKI, Masayuki et al. Study of dissolution mechanisms of nickel in sulfuric acid solution by electrochemical quartz crystal microbalance. *Corrosion Science*. 1997, 39(5), 901–911. doi: 10.1016/S0010-938X(97)81157-2.

[75]   QIU, Guihua et al. Polypyrrole-Fe3O4 magnetic nanocomposite prepared by ultrasonic irradiation. Macromolecular Materials and Engineering. 2006, 291(1), 68–74. doi: 10.1002/mame.200500285.

[76]   MILAKIN, Konstantin A. et al. Polypyrrole/gelatin cryogel as a precursor for a macroporous conducting polymer. *Reactive and Functional Polymers*. 2020, 157, 104751. doi: 10.1016/j.reactfunctpolym.2020.104751.

[77]   STEJSKAL, Jaroslav and PROKEŠ, Jan. Conductivity and morphology of polyaniline and polypyrrole prepared in the presence of organic dyes. *Synthetic Metals*. 2020, 264, 116373. doi: 10.1016/j.synthmet.2020.116373.

[78]   STEJSKAL, Jaroslav et al. Polypyrrole salts and bases: superior conductivity of nanotubes and their stability towards the loss of conductivity by deprotonation. *RSC Advances*. 2016, 6, 88382-88391. doi: 10.1039/c6ra19461c.

[79]   STEJSKAL, Jaroslav et al. Conducting polypyrrole-coated macroporous melamine sponges: A simple toy or an advanced material? *Chemical Papers*. 2021, 75, 5035–5055. doi: 10.1007/s11696-021-01778-8.

LIST OF FIGURES

LIST OF SYMBOLS AND ABREVIATIONS

CPC	conductive polymer composite
MPC	magnetic polymer composite
N_{agg}	aggregation number
EPT	electrical percolation threshold
CB	carbon black
CNT	carbon nanotubes
DPT	double percolation threshold
MC	Monte Carlo
FEM	finite element method
σ	conductivity
σ_m	conductivity of matrix
ρ	volume concentration
ρ_c	percolation threshold volume concentration
s	scaling parameter
σ_f	conductivity of filler
t	scaling parameter
SE_T	total shielding effectiveness
SE_A	shielding efficiency by absorption
SE_R	shielding efficiency by reflection
SE_M	shielding efficiency by multiple reflections
S_{11}	forward reflection coefficient
S_{21}	reverse transmission coefficient
R	reflectance
A	absorbance
T	transmittance
χ	magnetic susceptibility
LCST	lower critical solution temperature
ER	epoxy resin
PDMS	polydimethylsiloxane
E	Young modulus
ω	wetting coefficient

$\gamma_{i\text{-}j}$	interface tension of i-j interface
γ^p	polar contribution to overall surface tension
γ^d	dispersion contribution to overall surface tension
RVE	relative volume element
L_{RVE}	edge length of RVE
FEM	finite element method
PANI	polyaniline
PPy	polypyrrole
MS	melamine sponge
DGEBA	bisphenol A diglycidyl ether
DETA	diethylenetriamine
DCP	dicumyl peroxide
SEM	scanning electron microscopy
d	diameter
σ	standart deviation
t	thickness
SoA	size of aggregates
$J(x)$	current density vector
$S(x)$	spatially varying matrix conductivity
$E(x)$	vector of electric field
V	volume
M_s	saturation magnetization
M_r	remanent magnetization
H_c	coercivity
A	mechanical rigidity
B	mechanical compressibility

CURRICULUM VITAE

Personal information

Name	Marek Jurča
Address	Horní Lideč 336; 756 12
Telephone	739698675
E-mail	jurca@utb.cz
Nationality	Czech
Date of birth	06.03.1993

Education and training

Dates	2017–to date
Title of qualification awarded	Doctoral study – expected defence 2022
Principal branch	Nanomaterials and advanced materials
Organisation providing education	Centre of polymer systems – Tomas Bata University in Zlin

Dates	2015–2017
Title of qualification awarded	Ing.
	- *Received rector's award for excellent study results*
Principal branch	Polymer engineering
Organisation providing education	Faculty of technology – Tomas Bata University in Zlin

Dates	2012–2015
Title of qualification awarded	Bc.
	- *Received dean's award for excellent study results*
Principal branch	Polymer materials and technologies
Organisation providing education	Faculty of technology – Tomas Bata University in Zlin

LIST OF PUBLICATIONS

1. **JURČA M.**, VILČÁKOVÁ J., KAZANTSEVA N., PROKEŠ J., TRCHOVÁ M. and STEJSKAL J. Conducting and magnetic hybrid polyaniline/nickel composites. *Synthetic Metals*. 2022, 291, 117165. doi: 10.1016/j.synthmet.2022.117165.

2. **JURČA M.**, VILČÁKOVÁ J., GOŘALÍK M., MASAŘ M., PONÍŽIL P., KAZANTSEVA N., FOULGER S. H. and SÁHA P. Reduced percolation threshold of conductive adhesive through nonuniform filler localization: Monte Carlo simulation and experimental study. *Composites Science and Technology*. 2021, 214, 108964. doi: 10.1016/j.compscitech.2021.108964.

3. GOŘALÍK M., **JURČA M.**, BUBULINCA C., BABAYAN V., VILČÁKOVÁ J., KAZANTSEVA N., SÁHA P. Engineering Magnetic Type Radio-Absorbers Based on Composites with a Dual-Phase Polymer Matrix. *Electronic Materials Letters*. 2022, 18, 345–360. doi: 10.1007/s13391-022-00351-x.

4. BAUTKINOVÁ T., MAZÚR P., SOUKUPOVÁ G., DENDISOVÁ M., PROKEŠ J., **JURČA M.**, KOPECKÝ D., LHOTKA M., ULBRICH P. and HASSOUNA F. Tailor-made dual doping for morphology control of polyaniline chains in cellulose nanofiber-based flexible electrodes: electrical and electrochemical performance. *Journal of Materials Science*. 2022, 57, 13945–13961. doi: 10.1007/s10853-022-07491-3.

5. STEJSKAL J., VILČÁKOVÁ J., **JURČA M.**, FEI H., TRCHOVÁ M., KOLSKÁ Z., PROKEŠ J. and KŘIVKA I. Polypyrrole-Coated Melamine Sponge as a Precursor for Conducting Macroporous Nitrogen-Containing Carbons. *Coatings*. 2022, 12, 324. doi: 10.3390/coatings12030324.

6. FEI H., KAZANTSEVA N., PECHANCOVÁ V., **JURČA M.**, ŠKODA D., URBÁNEK M., MACHOVSKÝ M., BUGAROVÁ N. and SÁHA P. Effect of calcination temperature on electrochemical performance of niobium oxides/carbon composites. *Journal of Materials Science*. 2022, 57, 8504–8515. doi: 10.1007/s10853-022-06931-4.

7. ANJU, YADAV R. S., PÖTSCHKE P., PIONTECK J., KRAUSE B., KUŘITKA I., VILČÁKOVÁ J., ŠKODA D., URBÁNEK P., MACHOVSKÝ M., MASAŘ M., URBÁNEK M., **JURČA M.**, KALINA L. and HAVLICA J. High-Performance, Lightweight, and Flexible Thermoplastic Polyurethane Nanocomposites with Zn2+-Substituted CoFe2O4 Nanoparticles and Reduced Graphene Oxide as Shielding Materials against Electromagnetic Pollution. *ACS Omega*. 2021, 6(42), 28098–28118. doi: 10.1021/acsomega.1c04192.

8. STEJSKAL J., SAPURINA I., VILČÁKOVÁ J., **JURČA M.**, TRCHOVÁ M., KOLSKÁ Z., PROKEŠ J. and KŘIVKA I. One-Pot Preparation of Conducting Melamine/Polypyrrole/Magnetite Ferrosponge. *ACS Applied Polymer Materials*. 2021, 3(2), 1107-1115. doi: 10.1021/acsapm.0c01331.

9.   BANDERA Y., MCFARLANE T.M., BURDETTE M.K., **JURČA M.**, KLEP O. and FOULGER S.H. Synthesis of n-alkyl methacrylate polymers with pendant carbazole moieties and their derivatives. *Journal of Polymer Science: Part A Polymer Chemistry*. 2019, 57, 70-76. doi: 10.1002/pola.29285.

10.   VARGUN E., FEI H., WANG G., CHENG Q., VILČÁKOVÁ J., **JURČA M.**, BERGEROVÁ E., KAZANTSEVA N. and SÁHA P. Reduced Graphene Oxide-MWCNT Organogel Foam for Lithium-Sulfur Battery Cathode. *ECS Transactions*. 2019, 95(1), 81-87, doi: 10.1149/09501.0081ecst.

11.   YADAV R. S., KUŘITKA I., VILČÁKOVÁ J., MACHOVSKÝ M., ŠKODA D., URBÁNEK P., MASAŘ M., **JURČA M.**, URBÁNEK M., KALINA L. and HAVLICA J. NiFe2O4 Nanoparticles Synthesized by Dextrin from Corn-Mediated Sol–Gel Combustion Method and Its Polypropylene Nanocomposites Engineered with Reduced Graphene Oxide for the Reduction of Electromagnetic Pollution. *ACS Omega*. 2019, 4(26), 22069–22081. doi: 10.1021/acsomega.9b03191.

12.   MCFARLANE T. M., ZDYRKO B., BANDERA Y., WORLEY D., KLEP O., **JURČA M.**, TONKIN C., FOULGER S. H., VILČÁKOVÁ J., SÁHA P. and PFLEGER J. Design rules for carbazole derivatized n-alkyl methacrylate polymeric memristors. *Journal of Materials Chemistry C*. 2018, 6, 2533-2545. doi: 10.1039/c7tc05001a.

13.   VILČÁKOVÁ J., KUTĚJOVÁ L., **JURČA M.**, MOUČKA R., VÍCHA R., SEDLAČÍK M., KOVALČÍK A., MACHOVSKÝ M. and KAZANTSEVA N. Enhanced Charpy impact strength of epoxy resin modified with vinyl-terminated polydimethylsiloxane. *Journal of Applied Polymer Science*. 2017, 135(4), 45720. doi: 10.1002/app.45720.

OVERVIEW OF OTHER ACTIVITIES

Conferences:

JURČA M., GOŘALÍK M., VILČÁKOVÁ J., FOULGER S.H., MASAŘ M. and KAZANTSEVA N. (2019), Enhanced electrical conductivity of immiscible blends filled with nickel particles. *ACS National Meeting*, Orlando.

VARGÜN E., FEI H., WANG G., CHENG Q., VILČÁKOVÁ J., **JURČA M.**, BERGEROVA E., KAZANTSEVA N. and SÁHA P. (2019), Reduced Graphene Oxide-MWCNT Organogel Foam for Lithium-Sulfur Battery Cathode. *The Electrochemical Society ECS Transactions*, Brno.

JURČA M., BANDERA Y., MCFARLANE T. and FOULGER S. (2018), Polymer synthesis and characterization of methacrylate polymers with pendant carbazole group. *P.SAHA18 conference*, Zlín.

JURČA M., BANDERA Y., MCFARLANE T., MRHÁLEK O. and FOULGER S. (2017), Polymer synthesis and characterization of methacrylate polymers with pendant carbazole groups. *ACS National Meeting*, Washington.

MCFARLANE, T., BANDERA, I., ZDYRKO, B., **JURČA, M.**, KLEP, O., WORLEY, D. and FOULGER, S. (2017). Rational design of methacrylate polymers with pendant carbazole moieties for use as memristors. *ACS National Meeting*, Washington.

JURČA M., VILČÁKOVÁ J., KAZANTSEVA N. and BAŽANT P. (2016). Vliv dikumyl peroxidu na přípravu a vlastnosti epoxid-silikonových směsí. In Sborník konference *PLASTKO 2016*. Zlín: Univerzita Tomáše Bati ve Zlíně. ISBN 978-80-7454-590-0.

Work on projects:

TAČR, FW01010327: Pokročilé polymerní a kompozitní materiály pro aditivní výrobu, (2020–2024), member of research team.

MŠMT, INTER_EXCELLENCE, LTAUSA19066: A study of polymeric memristors based on methacrylate polymers with pendant carbazole moieties, (2020–2022), member of research team.

MŠMT, 8X20041 MSTC Danube, Design and preparation of multifunctional magnetic nanoparticles for cancer cell detection, (2020–2021), member of research team.

MŠMT, LTT20005 Spolupráce s asociací EASE na vývoji hybridního superkapacitoru (2020–2023), member of research team.

IGA/CPS/2021/002 – Preparation and characterization of nanocomposite systems – member of research team.

IGA/CPS/2020/003 – Preparation and characterization of nanoparticles for advanced applications – member of research team.

IGA/CPS/2019/007 – Development and study of conductive nanocomposite materials for electronic and electrotechnical applications – project leader.

IGA/CPS/2018/007 – Development and studies of conductive nanocomposite systems applicable in polymer electronics – member of research team.

Studies abroad:

Doctoral study at Material Science and Engineering department at Clemson University (South Carolina, USA), 01/2017–12/2017.

Freemover programme – Material Science and Engineering department at Clemson University (South Carolina, USA), 06/2016–07/2016.

Erasmus programme – Faculty of Chemistry and Chemical Technology at University of Ljubljana (SLO), 09/2014–01/2015.

Pedagogic activities:

Participation on teaching in laboratory classes of "The Basics of Food Packaging", TCPM/TP5ZB (FT, UTB).

Ing. Marek Jurča, Ph.D.

Multicomponent polymer systems with electromagnetic properties

Multikomponentní polymerní systémy s elektromagnetickými vlastnostmi